


# Modelling and treating *GRIN2A* developmental and epileptic encephalopathy in mice

Ariadna Amador,<sup>1,\*</sup> Christopher D. Bostick,<sup>1,\*</sup>  Heather Olson,<sup>2,3</sup> Jurrian Peters,<sup>2,3</sup> Chad R. Camp,<sup>4</sup> Daniel Krizay,<sup>1,5</sup> Wenjuan Chen,<sup>4,6</sup> Wei Han,<sup>4,7</sup> Weiting Tang,<sup>4,6</sup> Ayla Kanber,<sup>1</sup> Sukhan Kim,<sup>4</sup> Jiajie Teoh,<sup>1</sup> Megha Sah,<sup>1</sup> Sabrina Petri,<sup>1</sup> Hunki Paek,<sup>8</sup> Ana Kim,<sup>8</sup> Cathleen M. Lutz,<sup>8</sup> Mu Yang,<sup>1,9</sup> Scott J. Myers,<sup>4,10</sup> Subhrajit Bhattacharya,<sup>4</sup> Hongjie Yuan,<sup>4,10</sup> David B. Goldstein,<sup>1,5</sup> Annapurna Poduri,<sup>2,3</sup> Michael J. Boland,<sup>1,11</sup> Stephen F. Traynelis<sup>4,10</sup> and Wayne N. Frankel<sup>1,5</sup>

\*These authors contributed equally to this work.

NMDA receptors play crucial roles in excitatory synaptic transmission. Rare variants in *GRIN2A* encoding the GluN2A subunit are associated with a spectrum of disorders, ranging from mild speech and language delay to intractable neurodevelopmental disorders, including but not limited to developmental and epileptic encephalopathy. A *de novo* missense variant, p.Ser644Gly, was identified in a child with this disorder, and *Grin2a* knock-in mice were generated to model and extend understanding of this intractable childhood disease. Homozygous and heterozygous mutant mice exhibited altered hippocampal morphology at 2 weeks of age, and all homozygotes exhibited lethal tonic-clonic seizures by mid-third week. Heterozygous adults displayed susceptibility to induced generalized seizures, hyperactivity, repetitive and reduced anxiety behaviours, plus several unexpected features, including significant resistance to electrically-induced limbic seizures and to pentylentetrazole induced tonic-clonic seizures. Multielectrode recordings of neuronal networks revealed hyperexcitability and altered bursting and synchronicity. In heterologous cells, mutant receptors had enhanced NMDA receptor agonist potency and slow deactivation following rapid removal of glutamate, as occurs at synapses. NMDA receptor-mediated synaptic currents in heterozygous hippocampal slices also showed a prolonged deactivation time course. Standard anti-epileptic drug monotherapy was ineffective in the patient. Introduction of NMDA receptor antagonists was correlated with a decrease in seizure burden. Chronic treatment of homozygous mouse pups with NMDA receptor antagonists significantly delayed the onset of lethal seizures but did not prevent them. These studies illustrate the power of using multiple experimental modalities to model and test therapies for severe neurodevelopmental disorders, while revealing significant biological complexities associated with *GRIN2A* developmental and epileptic encephalopathy.

- 1 Institute for Genomic Medicine, Columbia University, New York, NY, USA
- 2 Epilepsy Genetics Program, Department of Neurology, Boston Children's Hospital, Boston, MA, USA
- 3 Department of Neurology, Harvard Medical School, Boston, MA, USA
- 4 Department of Pharmacology and Chemical Biology, Emory University, Atlanta, GA, USA
- 5 Department of Genetics and Development, Columbia University, New York, NY, USA
- 6 Department of Neurology, Xiangya Hospital, Central South University, Changsha, 410013, China
- 7 Department of Neurology, Children's Hospital of Chongqing Medical University, Chongqing, 400014, China
- 8 Department of Otolaryngology and Head and Neck Surgery, Columbia University, New York, NY, USA
- 9 Department of Psychiatry, Columbia University, New York, NY, USA
- 10 Center for Functional Evaluation of Rare Variants (CFERV), Emory University School of Medicine, Atlanta, GA, 30322, USA
- 11 Department of Neurology, Columbia University, New York, NY, USA

Received August 13, 2019. Revised March 6, 2020. Accepted March 25, 2020. Advance access publication June 24, 2020

© The Author(s) (2020). Published by Oxford University Press on behalf of the Guarantors of Brain. All rights reserved.

For permissions, please email: journals.permissions@oup.com

Correspondence to: Wayne N. Frankel  
 Institute for Genomic Medicine, Columbia University, New York, NY, USA  
 E-mail: wf2218@cumc.columbia.edu

**Keywords:** NR2A; autistic spectrum disorder; synaptic transmission; childhood epilepsy; experimental models

**Abbreviations:** DEE = developmental and epileptic encephalopathy; DIV = days *in vitro*; MEA = multielectrode array; NMDAR = N-methyl-D-aspartate receptor; PTZ = pentylenetetrazole

## Introduction

N-methyl-D-aspartate receptors (NMDARs) are ligand-gated ion channels involved in brain development and fast excitatory neurotransmission (Traynelis et al., 2010; Paoletti et al., 2013). These channels are heterotetramers composed of two obligate GluN1 subunits typically paired with two GluN2 subunits that are encoded by four genes, *GRIN2A*, *GRIN2B*, *GRIN2C* and *GRIN2D* (Traynelis et al., 2010; Paoletti et al., 2013). NMDARs can also form triheteromeric receptors through combinations of *GRIN1* and two different GluN2 subunits. Expression of these different complexes is spatially and temporally defined and varies among specific neuronal subtypes (Akazawa et al., 1994; Monyer et al., 1994; Bar-Shira et al., 2015). Each subunit contains a cytosolic carboxy terminal (CTD), a transmembrane region, an agonist binding domain (ABD), and an extracellular aminoterminal domain (ATD) that allow modulation of receptor activity and function. NMDARs are activated by binding of glycine and glutamate to GluN1 and GluN2, respectively, leading to opening of a cation selective pore. NMDARs undergo voltage-dependent channel block by extracellular  $Mg^{2+}$ , and depolarization can relieve  $Mg^{2+}$  block, allowing co-agonist activation to trigger  $Na^+$  and  $Ca^{2+}$  entry. The capacity of NMDARs to sense pre- and postsynaptic signals contributes to their critical role in synapse formation, development, and maintenance; they are thus key regulators of synaptic plasticity.

Pathogenic variants in *GRIN* genes have been associated with developmental and early onset epileptic encephalopathies (DEE) with accompanying co-morbidities, such as intellectual disability, autism, aphasia, and schizophrenia (Endele et al., 2010; Hamdan et al., 2011; de Ligt et al., 2012; Lesca et al., 2013; Petrovski and Kwan, 2013; Yuan et al., 2015; Hu et al., 2016; XiangWei et al., 2018). Data from 141 *GRIN2A* variants identified in patients (missense, nonsense, frameshift, splice site, duplication, translocation, and deletion variants) reveal a spectrum of phenotypes from mild to severe (Myers et al., 2019). Approximately 80% of variants are associated with a seizure phenotype and 71% with intellectual disability. Strehlow et al. (2019) report that more than 90% of *GRIN2A* patients have speech disorders, and that patients with missense mutations in the transmembrane domain and associated linkers have a poor prognosis, which constitutes about one-third of *GRIN2A* variants (XiangWei et al., 2018). This is consistent with genetic intolerance to variation of the transmembrane domain and linker regions

connecting the ABD, as evidenced by a paucity of missense variants in these regions in control populations (Ogden et al., 2017). Variants that do occur in these regions, such as P552R and P557R (Ogden et al., 2017), L812M (Pierson et al., 2014), M817V (Chen et al., 2017), and N615K (Endele et al., 2010), have been reported in patients with DEE. Furthermore, whole cell and single channel patch clamp recordings from cells with heterologous expression of mutant GluN2A receptors reveal gain-of-function via enhanced agonist potency and/or prolonged channel open times (Endele et al., 2010; Pierson et al., 2014; Ogden et al., 2017). These findings demonstrate the critical role of the transmembrane and linker domains in channel gating and suggest that other variants in this region could also result in altered receptor kinetics.

We describe a patient with DEE who presented with frequent infantile spasms and impaired development in the setting of the *GRIN2A* missense variant c.1930A>G, resulting in the amino acid substitution S644G in the highly conserved third transmembrane region (TM3). A combination of conventional anti-seizure medications and NMDAR antagonists were associated with a modest mitigation of seizures in the patient but no improvement of co-morbidities. We examined the variant in *Xenopus laevis* oocyte and HEK293 cell heterologous expression models and in a knock-in mouse model—including examination of both *in vivo* seizure and behaviour phenotypes, and primary neuronal network characteristics—while testing the efficacy of NMDAR blockers in each. Results from this extensive parallel *in vitro*, *in vivo*, and *ex vivo* genetic modelling approach provides first insight into the nature of *GRIN2A* gain-of-function disease and complementary means by which to test new therapies, while painting the picture of a complex neurodevelopmental disorder.

## Materials and methods

### Patient ascertainment and phenotyping

The patient was referred for consultation to the Epilepsy Genetics Program at Boston Children's Hospital (BCH) after clinical genetic testing for DEE revealed the *de novo* pathogenic variant. Consent was obtained to share de-identified patient data with collaborating researchers under a protocol approved by the Institutional Review Board (IRB). After discussion with the Office of Regulatory Affairs and IRB, the patient was

treated clinically with off-label memantine and dextromethorphan based on published reports of use for other indications and safety in children. The family was counselled that use of these medications was off-label. Clinical management with other medication and standard clinical monitoring with seizure counts, developmental assessment, and EEG continued as per standard of care.

## Mice, husbandry and genotyping

All mice were bred and procedures conducted at The Jackson Laboratory, Columbia University Irving Medical Center, or Emory University, each fully accredited by AAALAC, approved by respective IACUC and performed in accordance with state and federal Animal Welfare Acts and Public Health Service policies.

*Grin2a*<sup>S644G</sup> mice [official symbol: *Grin2a*<sup>em1(S644G)Frk</sup>] were generated in the C57BL/6NJ (B6NJ) mouse strain using CRISPR/Cas9 and an oligonucleotide donor sequence as part of the JAX Center for Precision Genetics (JCPG) and maintained by backcrossing heterozygous males to wild-type B6NJ females. For some experiments, as noted, male mutants were crossed with FVB/NJ females to generate cohorts of F<sub>1</sub> or F<sub>2</sub> hybrid mice. Mice were housed in ventilated cages at controlled temperature (22–23°C), humidity ~60%, and 12 h:12 h light:dark cycles. Mice had *ad libitum* access to regular chow and water. Mice were genotyped using the following PCR amplification primers (540-bp amplicon), using standard thermocycler conditions and Sanger sequenced (GeneWiz, Inc); F: CGAGTGTACACGCTGTGGAAATAG; R: TCAACCAGTGCTACAGAGTGATCT.

## Seizure studies

### Pup spontaneous seizure observation

Events in F<sub>2</sub> hybrids were recorded live using above-cage Sony HD digital cameras connected to a Samsung VCR set (Hanwha Techwin Co) for 24 h.

### Video-EEG

Electrode implantation of adult mice between 6 and 10 weeks of age was performed surgically, as previously described (Asinof *et al.*, 2016). Three silver wire electrodes were placed subdurally 1 mm rostral to bregma and 1 mm to either side of midline, and another over the cerebellum as reference. Signal was acquired on a Quantum 128 research amplifier (Natus, Inc). Differential and referential montages were examined in Neuroworks software (Natus).

### Electroconvulsive threshold

Tests on adult mice between 8 and 13 weeks of age were performed using transcorneal electrodes with the Ugo Basile Model 7801 electroconvulsive device as described previously (Asinof *et al.*, 2015). Settings for minimal or maximal generalized seizure end points were 299 Hz, 1.6 ms pulse width, 0.2 s duration, variable current; those for 6 Hz partial or psychomotor seizure end points were 6 Hz, 0.2 ms pulse width, 3.0 s duration, and variable current. Data were analysed as the integrated root mean square (iRMS, area under the curve) as (square root of Hz) × current × pulse width × duration.

## PTZ seizure susceptibility

Adult heterozygous and wild-type adult F<sub>1</sub> hybrid background mice of both sexes between 13 and 22 weeks of age were challenged with a threshold dose (45 mg/kg, determined empirically) of pentylenetetrazole (PTZ; Sigma-Aldrich, Co) in sterile phosphate-buffered saline (PBS). The mice were injected subcutaneously, placed onto clean bedding in a clear plastic box, and observed for at least 30 min. The incidence and latency to seizure end-point standards (Racine, 1972) was recorded and the tonic-clonic seizure end point—Racine score of 4—was used for analysis.

## Histology

Postnatal Day 14 pups were perfused transcardially using Bouin's solution. After perfusion the brains were carefully extracted, cut along the lambda-bregma points and were fixed in 4% (w/v) paraformaldehyde (PFA) in 0.1 M phosphate buffer at pH 7.4 overnight at 4°C. After serial dehydration steps, tissue was embedded in paraffin (Sigma, P3808) and sectioned at 5-µm thickness using Leica RM2125 microtome. Every 10th section was collected on a glass slide (Matsunami Glass, SUMGP14). Briefly, the slices were rehydrated and stained with haematoxylin then counterstained with eosin. These slices were subsequently dehydrated using ethanol and xylene and mounted with coverslip using Permount™ (Fisher Chemical, SP15-500). Images were acquired using a Nikon Eclipse E800M light microscope and NIS-elements software v4.51.

## RNA isolation and RT-qPCR

RNA from whole brains was extracted as previously described (Johnstone *et al.*, 2010). cDNA was synthesized using a qScript™ cDNA synthesis kit (Quanta BioSciences) using 1 µg per sample. Quantitative RT-qPCR was performed on a QuantStudio 5 (Applied Biosystems). Primers were designed using Primer3. Melt curve analyses were used to eliminate primer-dimer artefacts and check reaction specificity. All data were normalized to *Gapdh*. Primer sequences for selected targets: *Grin2b* – F: GAGCACGTGGACTTGACTGA; *Grin2b* – R: TACCACTCCGTGCTTATCGC; *Grin2a* – F: TCTTGAACCAAGCCCGGG; *Grin2a* – R: GCGAGTCAATCTGCCTC TT; PSD95 – F: ACCAAGATGAAGACACGCC; PSD95 – R: TCCGTTACCTGCAACTCAT; *Gapdh* – F: GACCACAGTCCATGCCATCAC; *Gapdh* – R: GTCCACCACCCTGTTGCTGTA

## Protein analysis

Crude membrane extracts were prepared by homogenizing cortices in 0.32 M sucrose, 1 mM NaHCO<sub>3</sub>, 1 mM MgCl<sub>2</sub>; and a protease inhibitor cocktail (ThermoScientific). Protein concentrations were determined by Bradford's method using bovine serum albumin (BSA) as standard. Samples (25 µg) were diluted in 4 × sodium dodecyl sulphate (SDS) protein gel loading dye, boiled for 5 min, separated on 10% Mini-PROTEAN TGX gel (Bio-Rad) and electroblotted to PVDF transfer membrane (Millipore). Non-specific binding was blocked for 30 min or 1 h at room temperature with 5% non-fat dry milk in Tween-Tris-buffered saline (TBS-T). Membranes were incubated overnight at 4°C with the following antibodies: NMDAR2A (Millipore, Cat# AB1555P), NMDAR2B (Cell Signaling, Cat# 4207S), all

normalized to Tubulin  $\beta$ -3 (BioLegend, Cat# 802001), PSD95 (Pierce or Synaptic Systems). Secondary antibodies anti-mouse and anti-rabbit (Cat# SA00001-1 and SA00001-2, Proteintech) were diluted at 1:10 000. All antibodies were prepared in 5% non-fat dry milk solution in TBS-T. Blots were developed using enhanced chemiluminescence ECL technique (Azure Biosystems, Inc, Model C400) and relative band densities were quantified using ImageJ software.

## Mouse neurobehavioural tests

All tests were done in adult mice between 8–16 weeks of age in the daytime when the lights were on, between 10 am and 4 pm. After testing and/or between trials, mice were gently returned to the home cage and the respective test apparatus was cleaned with 70% ethanol followed by water and wiped dry.

### Open field arena

Each mouse was placed gently in the centre of a clear Plexiglas arena ( $27.31 \times 27.31 \times 20.32$  cm) (Med Associates ENV-510) lit with dim light ( $\sim 5$  lx), and allowed to ambulate freely for 60 min. Infrared (IR) beams embedded along the  $x$ ,  $y$ -, and  $z$ -axes of the arena automatically track distance moved, horizontal movement, vertical movement, stereotypies, and time spent in the centre zone.

### Elevated plus maze

This test was conducted as previously described (Yang et al., 2012). The maze consists of two open arms ( $30$  cm  $\times$   $5$  cm) and two closed arms ( $30 \times 5 \times 15$  cm) extending from a central area ( $5 \times 5$  cm). Photo beams embedded at arm entrances register movements. Room illumination was  $\sim 30$  lx. Mice were placed in the centre, facing a closed arm and allowed to freely explore the maze for 5 min. Time spent in open and closed arms, the junction, and number of entries into each, were scored automatically by MED-PC V 64bit Software (Med Associates).

### Repetitive behaviours

Each subject was placed in an empty clean mouse cage, with a 0.25 cm layer of clean bedding lining the bottom. The cage was covered with a metal wire lid and a plastic filter top. Behaviours were recorded for 60 min and analysed using the time-sampling method for the last 10 min. An observation was scored every 30 s for a total of 20 samples. Occurrences of circling, hanging on the wire, backflipping, self-grooming, resting, and exploration were recorded for each sample.

### Acoustic startle response

Acoustic startle response was tested using the SR-Laboratory System (San Diego Instruments) as previously described (Yang et al., 2012). Test sessions began by placing the mouse in the Plexiglas holding cylinder for a 5-min

acclimation period. For the next 8 min, mice were presented with each of six trial types across six discrete blocks of trials, for a total of 36 trials. The intertrial interval was 10–20 s. One trial type measured the response to no stimulus (baseline movement). The others measured startle response to 40 ms sound bursts of 80, 90, 100, 110 or 120 dB. The six trial types were presented in pseudorandom order such that each was presented once within a block of six trials. Startle amplitude was measured every 1 ms over a 65 ms period beginning at the onset of the startle stimulus. The maximum startle amplitude over this sampling period was taken as the dependent variable. Background noise level of 70 dB was maintained over the duration of the test session.

## Auditory brainstem response

Mice were anaesthetized with ketamine (100 mg/kg, i.p.) and xylazine (10 mg/kg, i.p.). Auditory brainstem response (ABR) click test was performed in an acoustically and electrically shielded booth (Industrial Acoustic Company). The sound intensity level decreased from 80 to 5 dB at 5-dB intervals. The electrodes were placed subcutaneously on the vertex (active), mastoid (reference), and hindlimb (ground). The threshold was determined as the lowest intensity level that induced a detectable ABR response. Measurements were recorded and analysed with a S3 ABR system (Tucker Davis Technologies).

## Multielectrode array

### Primary neuron culture

Prior to use, 48-well multielectrode array (MEA) plates (Axion BioSystems) were coated overnight with 50  $\mu$ g/ml poly-D-lysine (Sigma) in 0.1 M borate buffer (pH 8.5). Cortices from postnatal Day 0 littermates were incubated in activated 20 U/ml Papain/DNase (Worthington) for 15 min at 37°C, centrifuged at 300g for 5 min, and washed in  $1 \times$  PBS. Cell pellets were suspended in NBA/B27 [consisting of Neurobasal<sup>TM</sup>-A (Life Technologies),  $1 \times$  B27 (Life Technologies),  $1 \times$  GlutaMAX<sup>TM</sup> (Life Technologies), 1% HEPES, and  $1 \times$  Penicillin/Streptomycin], supplemented with 1% foetal bovine serum (Gibco) and 5  $\mu$ g/ml laminin. Fifty thousand cells per well were plated on pre-coated MEA plates in a 40  $\mu$ l convex drop yielding a density of  $\sim 1600$  cells/mm<sup>2</sup>. The day after plating media was removed and replaced with pre-warmed NBA/B27. Cultures were maintained at 37°C in 5% CO<sub>2</sub>. Medium was 50% changed every other day with NBA/B27 starting on days *in vitro* (DIV)3.

### Multielectrode array data collection and analysis

Recordings were conducted prior to media change for 15 min per day using Axion BioSystems Maestro 768 channel amplifier and Axion Integrated Studios software (v2.4) at 37°C in a carbogen mixture of 95% O<sub>2</sub>, 5% CO<sub>2</sub>. A Butterworth band-pass filter (200–3000 Hz) and an adaptive



threshold spike detector set at  $7\times$  the standard deviation (SD) of noise to record raw data and spike list files. Data were analysed using the meaRtools package (Gelfman *et al.*, 2018). Spike list files were used to extract additional spike, burst, and network features. At least 5 spikes/min per electrode were required; wells with fewer than four active electrodes for more than 30% of the total recording days were discarded, resulting in 94% of wells and 94% of electrodes over seven 48-well MEA plates deemed active.

### Burst detection

The maximum interval burst detection algorithm (Neuroexplorer software, Nex Technologies) was used. Based on previous studies (Johnstone *et al.*, 2010; Mack *et al.*, 2014), we required that a burst consist of at least five spikes, lasting at least 50 ms, and that the maximum duration between two spikes within a burst was 0.05 s. Adjacent bursts were merged if the duration between them was  $<0.11$  s.

### Network burst detection

Spike time within spike trains from all electrodes in a well was normalized using a bin size of 2 ms to guarantee that—at most—one spike is called within each bin. A Gaussian filter was applied to smooth the binned spike train from each electrode. The smoothed signal was then standardized to a maximum value of 1. The sum of all smoothed signals from individual electrodes were then smoothed again using the same Gaussian filter before applying the Otsu global thresholding method (Otsu, 1975) to the signal from each well to automatically detect burst intervals. Network bursts were analysed in 400 ms windows. Mutual information was calculated as previously described (Gelfman *et al.*, 2018).

### Electrical stimulation

After DIV25, two electrodes per well (370  $\mu\text{m}$  apart) were probed with 10 biphasic 0.2 Hz pulses sequentially to investigate evoked electrical responses. Evoked responses were measured with a pulse amplitude fixed at 1.6–2.0 V peak-to-peak with the positive phase coming before the negative phase, and lasting for 200  $\mu\text{s}$  per phase (Wagenaar and Potter, 2004; Wagenaar *et al.*, 2004). Peristimulus time histograms (PSTH) were generated using the Axion BioSystems Neural Metric Tool (v2.2.4). A PSTH for each well was calculated by recording the spiking activity over a 400 ms period after each stimulation (20 stimuli per well) then averaging the number of spikes on active electrodes ( $>0.1$  Hz) in the well per trial for each histogram bin (1 ms) (Shahaf and Marom, 2001).

## Two-electrode voltage clamp and whole-cell voltage clamp recordings

The cDNAs for wild-type human NMDA receptor subunits GluN1-1a [hereafter GluN1 (NCBI NM\_007327/NP\_015566)] and GluN2A (NCBI NM\_000833/NP\_000824) were subcloned into pCI-neo (Promega). Site-

directed mutagenesis was performed to generate human GluN2A-S644G construct as previously described (Yuan *et al.*, 2015). Preparation and injections of cRNA, TEVC from *Xenopus laevis* oocytes, and expression of triheteromeric receptors were performed as previously described (Hansen *et al.*, 2014). The cDNAs encoding wild-type and mutant GluN2A subunits were fused at the C-terminal with a synthetic linker, a coiled-coil domain C1 or C2, and an ER retention signal, as previously described (Hansen *et al.*, 2014). Complementary RNAs encoding GluN1, as well as C1- and C2-tagged GluN2A, were injected at a 1:2:2 ratio with  $\sim 10$  ng total cRNA at a total volume of 50 nl (1:2:2 for GluN1: GluN2A<sub>C1</sub>: GluN2A<sub>C2</sub>, or GluN1: GluN2A<sub>C1</sub>-S644G: GluN2A<sub>C2</sub> or GluN1: GluN2A<sub>C1</sub>-S644G: GluN2A<sub>C2</sub>-S644G) and were kept at 19°C in Barth's solution for 1–3 days before recording. For all experiments, the cRNA was diluted with RNase-free water. Barth's solution contained (in mM) 88 NaCl, 2.4 NaHCO<sub>3</sub>, 1.0 KCl, 0.33 Ca(NO<sub>3</sub>)<sub>2</sub>, 0.41 CaCl<sub>2</sub>, 0.82 MgSO<sub>4</sub>, and 5 Tris/HCl (pH 7.4). Glutamate and glycine concentration-response curves were recorded at  $-40$  mV holding potential. Magnesium and drug inhibition curves were recorded at  $-60$  mV, and zinc inhibition curves were recorded at  $-20$  mV (pH 7.3, Yuan *et al.*, 2014). The oocyte recording solution contains (in mM) 90 NaCl, 1 KCl, 10 HEPES, 0.5 BaCl<sub>2</sub>, and 0.01 EDTA (pH 7.4). HEK293 cells were maintained and transfected with GFP, GluN1, and GluN2A-wild-type, GluN2A-S644G, GluN2A<sub>C1</sub>, GluN2A<sub>C2</sub>, GluN2A<sub>C1</sub>-S644G, and/or GluN2A<sub>C2</sub>-S644G using the calcium phosphate method, as previously described (Chen and Okayama, 1987; Hansen *et al.*, 2014; Yuan *et al.*, 2014; Chen *et al.*, 2017). The cDNA transfection ratios for GluN1: GluN2: GFP were 1:1:5 and for GluN1:GluN2<sub>C1</sub>:GluN2<sub>C2</sub>:GFP were 1:1:1:1; all cDNAs were at 0.2  $\mu\text{g}/\mu\text{l}$ , and 2.5  $\mu\text{l}$  added to each well, which held 0.5 ml of media. Whole-cell voltage clamp were performed with a rapid solution exchange system and analysed by ChannelLab as previously described (Yuan *et al.*, 2014; Ogden *et al.*, 2017).

## Hippocampal whole-cell patch clamp recordings

Horizontal hippocampal brain slices (300  $\mu\text{m}$ ) were made from postnatal Day 13–17 wild-type (+/+) and S644G/+ littermate F<sub>2</sub> hybrid mice of both sexes using a vibratome (TPI). During preparation, the slices were bathed in an ice-cold (0–2°C) sucrose-based artificial CSF containing (in mM) 230 sucrose, 24 NaHCO<sub>3</sub>, 10 glucose, 2.5 KCl, 1.25 NaH<sub>2</sub>PO<sub>4</sub>, 10 MgCl<sub>2</sub>, and 0.5 CaCl<sub>2</sub> bubbled with 95% O<sub>2</sub>/5% CO<sub>2</sub>. After preparation, slices were transferred to a NaCl-based recovery artificial CSF containing (in mM) 130 NaCl, 24 NaHCO<sub>3</sub>, 10 glucose, 2.5 KCl, 1.25 NaH<sub>2</sub>PO<sub>4</sub>, 4 MgCl<sub>2</sub>, and 0.5 CaCl<sub>2</sub> bubbled with 95% O<sub>2</sub>/5% CO<sub>2</sub>. The recovery solution was supplemented with 30  $\mu\text{M}$  7-chlorokynurenic and incubated at 32°C for 30 min before

returning them to room temperature and left to recover for at least 1 h prior to use.

Evoked CA1 pyramidal cell EPSCs were recorded at room temperature in artificial CSF but with 0.2 mM MgCl<sub>2</sub>, 1.5 mM CaCl<sub>2</sub>, and no 7-chlorokynurenic acid. Thin-walled borosilicate glass (1.5-mm outer, 1.12-mm inner diameter, WPI Inc) was used to fabricate recording electrodes (4–6 MΩ), which were filled with (in mM) 100 Cs-gluconate, 5 CsCl, 0.6 EGTA, 5 BAPTA, 5 MgCl<sub>2</sub>, 8 NaCl, 2 Na-ATP, 0.3 Na-GTP, 40 HEPES, 5 Na-phosphocreatine, and 3 QX-314. Membrane resistance was on average 252 ± 39 (+/+ ) and 234 ± 36 MΩ (+/S644G), series resistance was on average 15 ± 1.1 (+/+ ) and 18 ± 1.6 MΩ (+/S644G), and cell capacitance was 116 ± 5.9 (+/+ ) and 117 ± 9.3 pF (+/S644G). Monosynaptic release of glutamate was evoked at 0.033 Hz using a monopolar tungsten-stimulating electrode by injecting 50–150 μA of current for 0.1 ms along the Schaffer collateral pathway. CA1 pyramidal cells were held at –30 mV to minimize magnesium block. The NMDAR-mediated current component was isolated via bath application of 10 μM NBQX (AMPA antagonist, Sigma) and 10 μM gabazine (GABA<sub>A</sub>R antagonist, Sigma). Cells were held in 10 μM NBQX and 10 μM gabazine for 10 min before baseline current responses were recorded. A total of eight epochs were recorded and averaged together. At the conclusion of recording, 200 μM DL-APV (Sigma) was applied to ensure responses were mediated via NMDARs; DL-APV caused a similar change in the baseline leak current of –17 ± 3.2 (+/+ ) and –18 ± 7.7 pA (+/S644G).

Recordings were made using an Axopatch 1D amplifier (Molecular Devices), digitized at 20 kHz using a Digidata 1440a and Axon pClamp10 software, and filtered at 5 kHz using an eight-pole Bessel filter (–3 dB; Frequency Devices). Series resistance was monitored throughout the experiment and was typically 8–20 MΩ. Cells were excluded from analysis if they did not meet all of the following: membrane capacitance >90 pF, membrane resistance higher than 100 MΩ, access resistance <25 MΩ, <20% change in access resistance for the duration of the experiment, and a leak current less than –200 pA. All data were analysed offline with ChanneLab (Synaptosoft), using a dual-exponential function with the following settings: peak average points = 3, number of fit points = 400, number of parse points = 200, number of iterations = 900, number of restarts = 2, offset = fixed, baseline duration = 50 ms, and start scan at 10 ms previous of the initial downward deflection at the start of the EPSC.

## Pharmacology

Dimethyl sulfoxide (DMSO) was from Fisher Scientific, NMDA was from Tocris, radiprodil was from Cayman Chemical, and memantine and dextromethorphan were from Sigma-Aldrich. For use in MEA, stock solutions of 1000× and the final desired concentration were prepared for each compound in deionized water (NMDA 100 mM, dextromethorphan and memantine 50 mM). MEA plates were dosed by addition of 5 μl of appropriately diluted stock

concentration of drug to a parallel dosing plate, then half (150 μl) of the media from the MEA plate was removed and added to the parallel dosing plate and mixed prior to adding the media back to the MEA plate. Plates were allowed to equilibrate briefly (2–3 min) post-administration of drug prior to recording and non-treated wells were used to verify stabilization was achieved. Concentration–response relationships were determined in a cumulative manner, in which the concentration of drug present in the medium was increased in a stepwise manner (Novellino et al., 2011).

For subcutaneous delivery in mice, dextromethorphan was administered in a 0.9% saline vehicle (at 25 mg/kg). Formulation to dissolve radiprodil consisted of 2% N,N-dimethylacetamide (DMA, Sigma)/10% propylene glycol (PG, Sigma)/30% 2-hydroxypropyl-beta-cyclodextrin (HPBCD, Sigma). Quinidine (Sigma Aldrich) was diluted in saline solution and administered at 10 mg/kg. Dissolved radiprodil was diluted in saline solution and administered at 2 mg/kg. Nuedexta<sup>®</sup> was prepared as a formulation of 25:10 mg/kg dextromethorphan:quinidine.

## Statistical analyses

For animal studies, the non-parametric Mann-Whitney rank-sum test was performed when data were not normally distributed or when fewer than 10 animals were available per group and another test was not more appropriate. Two-way repeated measures ANOVA was used for open field arena tests. Survival curves were analysed using the Mantel-Cox log-rank test. A non-parametric mixed-model log-Poisson test was done for cortical layer cell counts from both hemispheres. Steel-Dwass test with correction for multiple comparisons was used for hippocampal morphometry from both hemispheres. Two-sample, two-tailed Student's *t*-test was used for *in vitro* electrophysiology, including data analysed from acute hippocampal slices. For MEA neuron culture spontaneous phenotypes, data were rank and normal quantile transformed, a least squares regression model performed, *P*-values for each DIV were obtained for plate ID and genotype effects, the latter were adjusted by Bonferroni correction for the 11 DIV measurements per feature, and for DIVs with significant genotype effects, the significance between each homozygous or heterozygous against wild-type was determined by a *post hoc* Dunnett's test set at *P* < 0.05. For MEA drug responses, data were transformed as above and genotype × treatment interaction effects were tested in a least-squares regression model. For experiments where multiple statistical analyses were performed on the same dataset, our significance threshold was lowered to correct for family-wise error rate (FWER). All studies were designed so that an effect size of at least 1.6 was detected at 80% or greater power.

## Data availability

The data that support the findings of this study are available from the corresponding author, upon reasonable request.

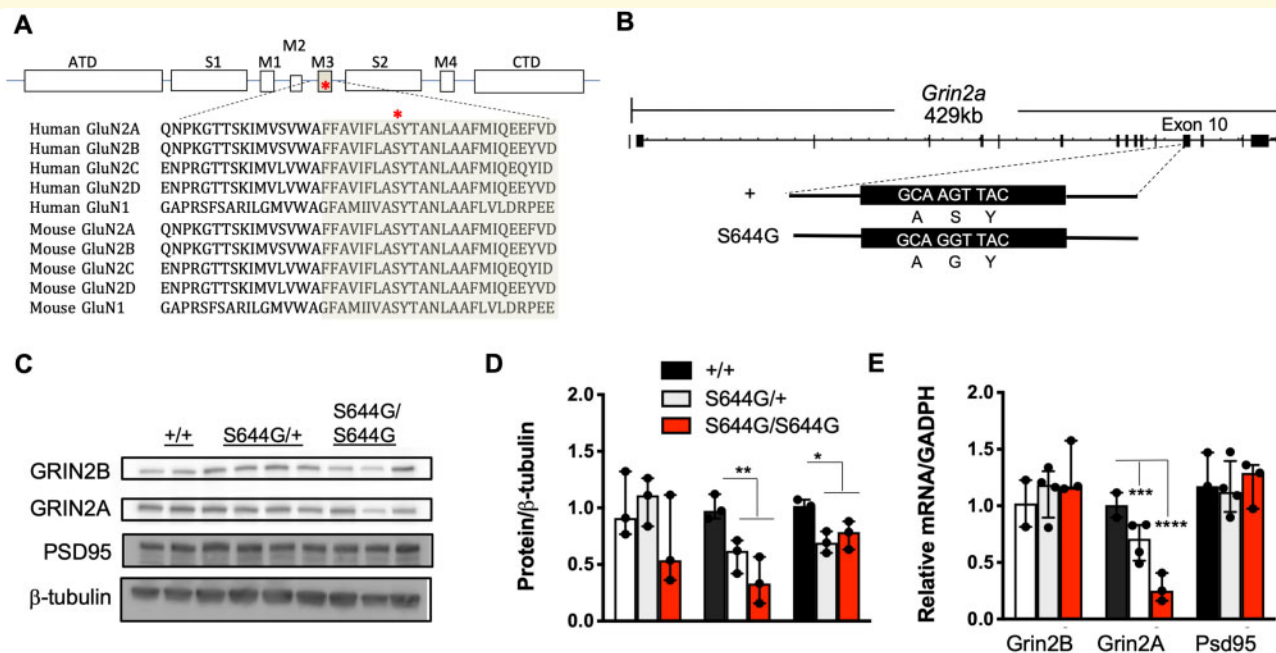


**Figure 1** *GRIN2A* S644G substitution in human and in mouse model. **(A)** Alignment of the GluN2A protein sequence across human and mouse GluN subunits. The TM3 transmembrane domain is highly conserved within the NMDAR family, including the serine residue that appears mutated in the patient. ATD = amino terminal domain; S1 and S2 = polypeptide chains that form the agonist-binding domain (ABD); M1, M2, M3, and M4 = transmembrane domain (TM) helices 1, 3, and 4, and the membrane re-entrant loop 2; CTD = carboxy-terminal domain (COOH). **(B)** Structure of the mouse *Grin2a* gene and A > G nucleotide mutation that results in serine to glycine amino acid substitution induced by CRISPR/Cas9 mutagenesis creating the S644G allele from wild-type. **(C)** Western blot of whole brain lysates probed for GluN2B, GluN2A, PSD95,  $\beta$ -tubulin ( $n = 3$ ). **(D)** Plot of the amount of protein normalized to  $\beta$ -tubulin and wild-type. **(E)** Expression quantification of total *GRIN2B*, *GRIN2A*, and *PSD95* mRNA was determined by qRT-PCR and normalized to the housekeeping gene, *GADPH*;  $n = 3$ . Error bars are standard error of the mean (SEM). \* $P < 0.05$ ; \*\* $P < 0.01$ ; \*\*\* $P < 0.001$ ; \*\*\*\* $P < 0.0001$ . Student's *t*-test.

## Results

### A *de novo* *GRIN2A* variant in a child with developmental and epileptic encephalopathy

#### Clinical presentation and aetiology

A 4-month-old male presented with concerns for visual tracking and developmental delay and developed seizures at 6–8 months. There were no risk factors for epilepsy nor family history of epilepsy. Prenatal history was notable for polyhydramnios and preterm labour at 32 weeks gestation, and birth was at 36 weeks gestation by Caesarean section. He required minimal resuscitation with Apgar scores of 3, 5, and 8 at 1, 5 and 10 min, respectively, and was monitored in neonatal intensive care for 2 days for feeding and swallowing concerns. MRI at 7 months was normal.

At 6–8 months the boy exhibited ~200 seizures per month consisting initially of clusters of myoclonic seizures that evolved to infantile spasms. Other seizure types

eventually observed included focal motor (tonic) seizures, focal impaired awareness seizures, generalized tonic seizures, and generalized tonic-clonic seizures. EEG recordings were consistent with epileptic encephalopathy, including diffuse background slowing and disorganization, electroclinical seizures, some with generalized and some with focal onset, and interictal generalized spike-slow wave complexes and multifocal spikes. He had profound global developmental delay without regression, cortical visual impairment, spastic quadriplegia, and oropharyngeal dysphagia warranting exclusive gastrostomy feeding. At 6 years of age, he continues to be non-verbal and non-ambulatory with limited purposeful hand use and lack of independent head control. Together, his features constitute a DEE.

Molecular diagnosis via exome sequencing identified the *de novo* heterozygous missense variant c.1930A>G in the *GRIN2A* gene encoding the GluN2A NMDAR subunit. The resulting *GRIN2A* S644G amino acid substitution resides in the transmembrane domain TM3, an area with high sequence conservation across all NMDAR genes in human and mouse (Fig. 1A).

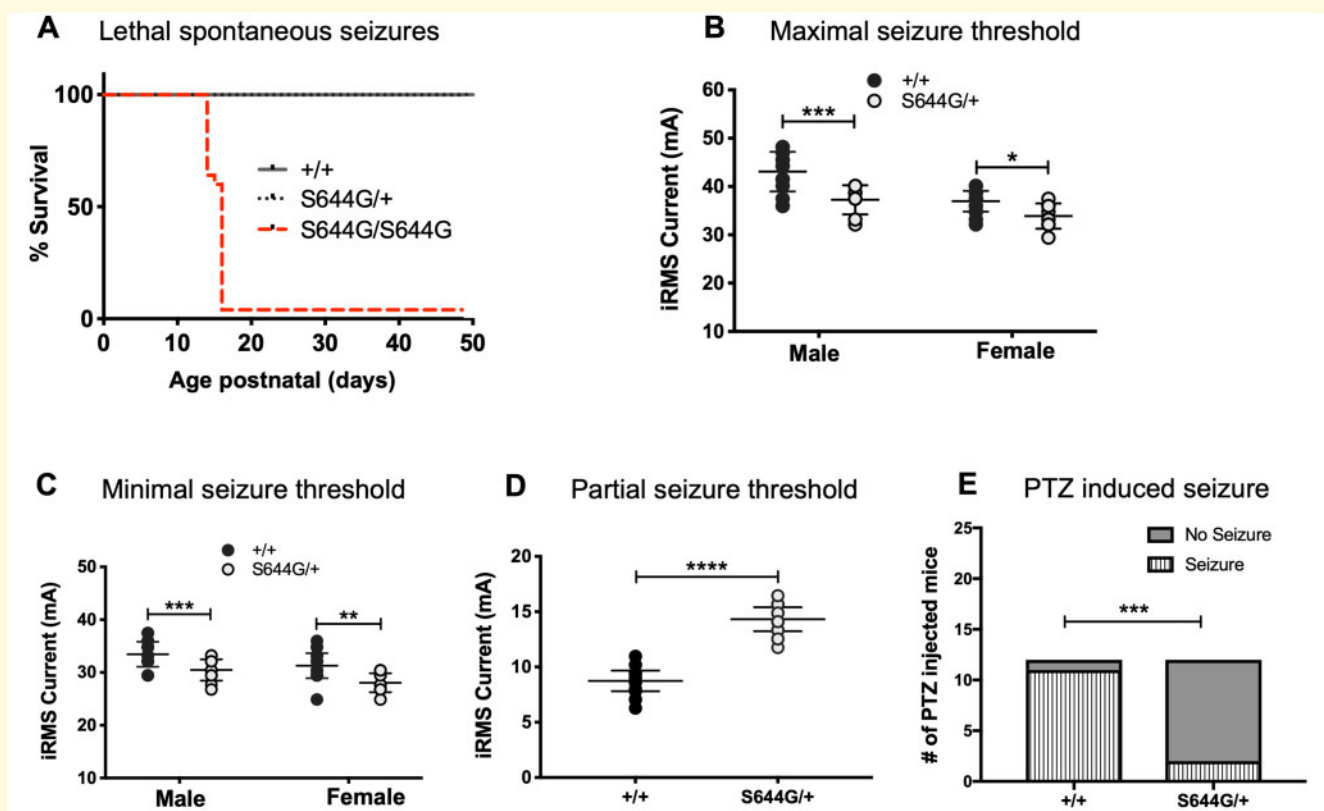


**Figure 2** Seizure susceptibility of *Grin2a*<sup>S644G</sup> mice. (A) Survival curve showing the rate and onset between postnatal Days 15 and 17 of S644G genotype-dependent in F<sub>2</sub> hybrid male and female mice. (B and C) Heterozygous (het) adult mice have lower seizure threshold in minimal seizure end points (female: *n* = 20 wild-type, *n* = 22 het, *P* = 0.0048; male: *n* = 31 wild-type, *n* = 27 het, *P* = 0.0035); and maximal seizure ECT end-points (female: *n* = 6 het, *n* = 7 wild-type; *P* = 0.0434; male: *n* = 15 het, *n* = 9 wild-type; *P* = 0.0007), but (D) are significantly more resistant to partial seizures in the 6 Hz ECT test (sexes combined: *n* = 33 het, *n* = 31 wild-type; *P* =  $4.1 \times 10^{-12}$ ); Mann-Whitney rank-sum test. (E) Significantly decreased tonic-clonic seizure incidence in S644G/+ mice (*n* = 12; five males, seven females) compared to wild-type mice (*n* = 12; six males, six females) following subcutaneous injection of 45 mg/kg PTZ (*P* = 0.0006, two-tailed Fisher's exact test). Error bars are quartiles. \**P* < 0.05; \*\**P* < 0.01; \*\*\**P* < 0.001; \*\*\*\**P* < 0.0001. iRMS = integrated root mean square.

## *Grin2a*<sup>S644G</sup> mutant mice have unusual seizure, behaviour and histopathological features

*Grin2a* knockout mice with abnormal developmental features and mild epileptiform activity have been reported (Salmi et al., 2018, 2019), but the features of mice carrying *Grin2a* putative gain-of-function variants modelling DEE were not yet described. To model S644G we generated a mouse line carrying the orthologous mutation on the B6NJ strain background (Fig. 1B). B6NJ *Grin2a*<sup>S644G/+</sup> (S644G/+) females are fertile and had no difficulties delivering, but did not care for the pups beyond the first postnatal day, resulting in no surviving pups of any *Grin2a* genotype (Supplementary Table 1). Observational assessments including pup retrieval, self-grooming and pup care suggested impaired maternal behaviours in B6NJ S644G/+ females.

To study homozygous mutants, F<sub>2</sub> hybrid mice were generated from an intercross between (FVB/NJ × B6NJ-S644G)F<sub>1</sub> parents. Although all *Grin2a* genotypes survived to the third

week, all S644G homozygotes unexpectedly died of a lethal seizure between postnatal Days 15 and 17 (Fig. 2A). Evidence for seizure included maximal hindlimb extension, observed both in carcasses and in animals immediately prior to death. Seizures began suddenly with a wild run followed rapidly by a tonic-clonic phase and ultimately maximal tonic hindlimb extension, which was terminal. The early third week onset correlates with the known temporal peak of *Grin2a* expression (Bar-Shira et al., 2015). Heterozygous animals did not have a shortened lifespan and exhibited neither behavioural seizures during routine handling, nor epileptiform activity during continuous video-EEG analysis (Supplementary Fig. 1).

Seizure susceptibility of S644G/+ adults was assessed using electroconvulsive threshold (ECT) testing targeting minimal clonic (forebrain), maximal tonic (hindbrain/brainstem), and psychomotor seizure (6 Hz test) end points. Heterozygous S644G/+ mice exhibited a decreased seizure threshold (i.e. relatively susceptible) to both minimal and maximal electroconvulsive end-points, (Fig. 2B and C), but in the 6 Hz seizure test showed a highly significantly



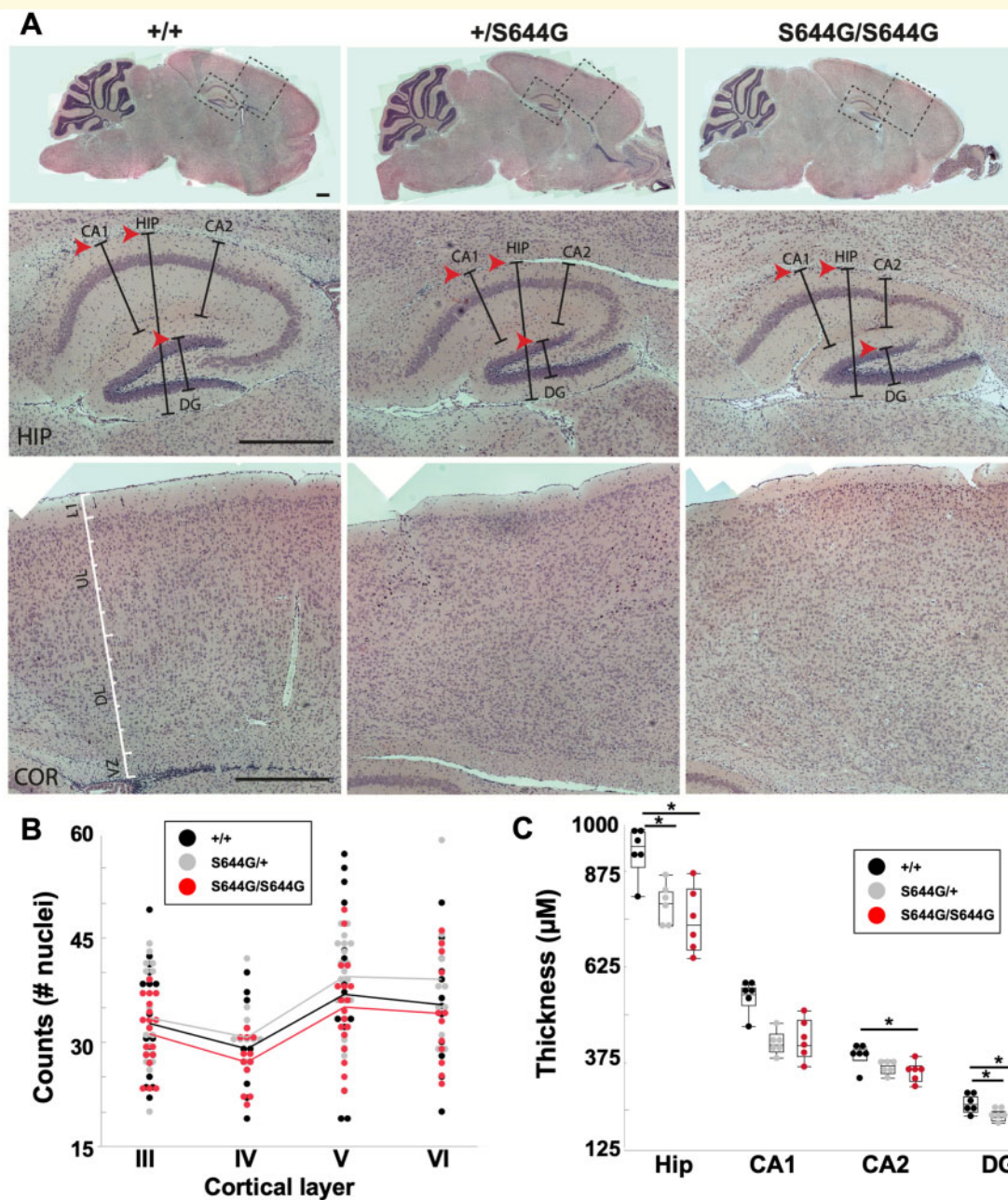


**Figure 3** Aberrant hippocampal morphology of *Grin2a*<sup>S644G</sup> adolescent mice. **(A)** Haematoxylin and eosin stained brain sections (scale bars = 500 µm). At postnatal Day 14, markedly decreased hippocampal thickness, particularly in CA1 and DG (arrowheads). **(B)** Cerebral cortex, showing no consistent significant differences in width between genotypes, proxied by cell counts per layer after accommodating random variation between replicates. **(C)** Decreased thickness in the hippocampus, particularly in CA1 and DG.  $n = 3$  for each genotype, counts or thickness measured from both hemispheres. Error bars are quantiles.  $*P < 0.05$ ; Steel-Dwass non-parametric means comparison.

increased threshold (i.e. relatively resistant), suggesting significant abnormality in the limbic system (Fig. 2D). Heterozygotes were also relatively resistant to PTZ induced tonic-clonic seizures (Fig. 2E).

*Grin2a* mRNA and protein were present but modestly decreased in heterozygous and homozygous pups at postnatal Day 14, as was the scaffold PSD95 protein but not its transcript (Fig. 1C–E). *Grin2a* is expressed highly in

the hippocampus and we detected thinning of the dentate gyrus and CA1 region as a common feature of S644G heterozygotes and homozygotes compared to age-matched wild-type (Fig. 3). We did not detect gross changes in cortical lamination. Since *Grin2a* expression is predominantly postnatal, together these results suggest the likelihood of hippocampal cellular atrophy prior to postnatal Day 14.

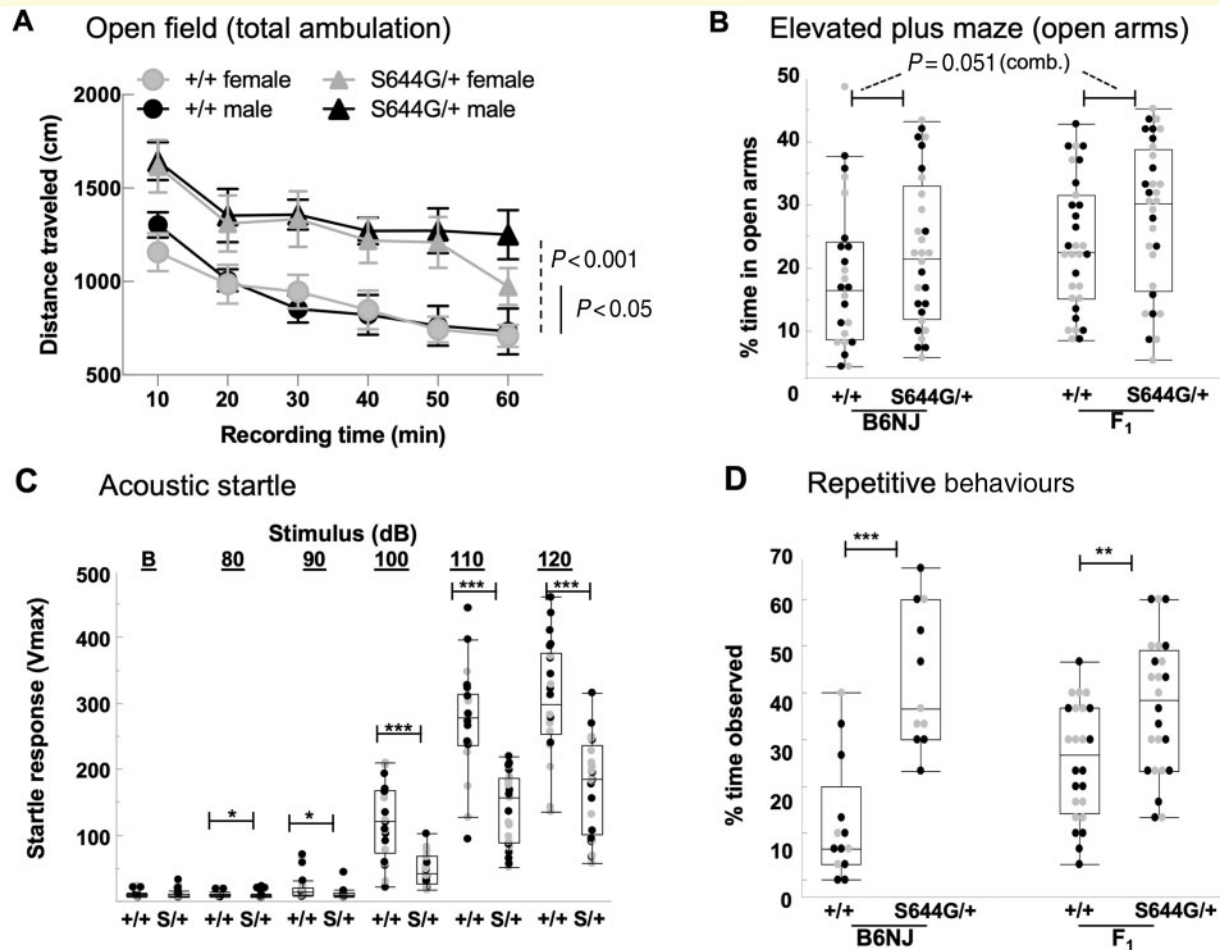


**Figure 4 Behavioural phenotypes in *Grin2a*<sup>S644G/+</sup> mice.** (A) Distance travelled in the open field was increased in both sexes of S644G/+ mice compared with +/+ (B6NJ background shown; females  $n = 9$  +/+, 13 S644G/+; males  $n = 12$  +/+, 12 S644G/+). (B) In the elevated plus maze test the per cent time spent on the open arms had a trending increase in S644G/+ mice when both B6NJ and F<sub>1</sub> hybrid data backgrounds were combined ( $P = 0.051$ , Mann-Whitney rank-sum test). (C) S644G/+ (S/+) mice exhibited a significantly decreased acoustic startle response to 90–120 dB stimuli (B6NJ background shown,  $n = 22$  +/+,  $n = 25$  S/+). (D) S644G/+ mice exhibited increased repetitive behaviours (back flipping and grooming events) on each strain background ( $n = 12$  +/+,  $n = 11$  S644G/+). Error bars are SEM for A and quartiles for B–D. Females are grey and males are solid markers \* $P < 0.05$ ; \*\* $P < 0.01$ ; \*\*\* $P < 0.001$ ; \*\*\*\* $P < 0.0001$ .

We performed a battery of neurobehavioural tests in adult littermates on B6NJ and F<sub>1</sub> hybrid backgrounds. In the open field, B6NJ S644G/+ heterozygotes of both sexes showed increased ambulation compared to wild-type (Fig. 4A), but in F<sub>1</sub> hybrids only females displayed this phenotype (data not shown). In the elevated plus maze, S644G/+ mice of both backgrounds trended towards more time on the open arms, while showing no difference in total arm entries or time at the junction (data not shown), suggestive of decreased anxiety-like behaviour (Fig. 4B).

Heterozygotes of both sexes exhibited a significantly reduced acoustic startle response (B6NJ, Fig. 4C; F<sub>1</sub>, data not shown) despite mice of both genotypes having auditory brainstem response thresholds of 20 dB sound pressure level, indicating that hearing was not impaired *per se*

but that the response to stimulus was altered. Because NMDAR mutations are associated with autism spectrum disorder (Hacohen et al., 2016; Grea et al., 2017; Rossi et al., 2017) and repetitive behaviour in mice (Lee et al., 2015; Kim et al., 2019), we evaluated repetitive behaviours using established criteria for rodents (see ‘Materials and methods’ section). S644G/+ heterozygotes of both sexes and strain backgrounds exhibited a significant increase in repetitive behaviours, which included vertical jumping, backflips and self-grooming (Fig. 4D). Together with impaired maternal care, the neurobehavioural features of S644G/+ mice suggest a complex neurological phenotype, with the most prominent features being hyperactivity, decreased anxiety-like behaviour, and repetitive behaviours.

**Table 1** Functional properties of diheteromeric GluN1/GluN2A-S644G NMDARs

|   | hGluN2A / hGluN2A    | hGluN2A-S644G / hGluN2A-S644G        |
|---|----------------------|--------------------------------------|
| <b><i>Xenopus laevis</i> oocytes</b>      |                      |                                      |
| Glu, EC <sub>50</sub> (μM)                | 3.0 (2.5, 3.5; 10)   | 0.18 (0.15, 0.20; 12) <sup>a</sup>   |
| Gly, EC <sub>50</sub> (μM)                | 0.86 (0.55, 1.1; 12) | 0.08 (0.047, 0.094; 14) <sup>a</sup> |
| Mg <sup>2+</sup> , IC <sub>50</sub> (μM)  | 26 (17, 31; 11)      | 33 (27, 35; 26)                      |
| pH, IC <sub>50</sub>                      | 7.02 (6–17)          | 5.86 (8–17)                          |
| Current pH 6.8 / pH 7.6 (%)               | 44 ± 1.3 (8)         | 99 ± 0.07 (8) <sup>a</sup>           |
| Zn <sup>2+</sup> IC <sub>50</sub> (nM)    | 23 (6.7, 28; 9)      | ND                                   |
| Inhibition by 300 nM Zn <sup>2+</sup> (%) | 56 ± 4.2 (9)         | 8.1 ± 1.6 (8) <sup>a</sup>           |
| P <sub>OPEN</sub> (from MTSEA)            | 0.15 ± 0.01 (13)     | 1.0 ± 0.29 <sup>a</sup> (20)         |
| <b>HEK-293 cells</b>                      |                      |                                      |
| Amplitude (peak, pA/pF)                   | 70 ± 15 (5)          | 194 ± 81 (7)                         |
| Amplitude (SS, pA/pF)                     | 46 ± 9.1 (5)         | 81 ± 27 (7)                          |
| Current (SS) / Current (Peak)             | 0.70 ± 0.04 (5)      | 0.57 ± 0.13 (7)                      |
| 10–90% Rise time (ms)                     | 9.0 ± 1.2 (5)        | 8.5 ± 0.9 (7)                        |
| τ <sub>FAST</sub> deactivation (ms)       | 25 ± 6.3 (5)         | 1077 ± 292 (7)                       |
| τ <sub>SLOW</sub> deactivation (ms)       | 503 ± 223 (5)        | 3265 ± 1022 (7)                      |
| τ <sub>FAST</sub> amplitude (%)           | 90% (5)              | 67% (7)                              |
| τ <sub>W</sub> deactivation (ms)          | 48 ± 4.7 (5)         | 2129 ± 608* (7)                      |
| Charge transfer (pA ms/pF)                | 3454 (5)             | 173 518 (7)                          |

Potency data are mean (95% confidence interval determined from logEC<sub>50</sub>; n).

<sup>a</sup>Non-overlapping confidence intervals.

Agonist concentration–response curves were fitted by:

$$\text{Response (\%)} = 100 / (1 + (\text{EC}_{50} / [\text{concentration}])^N)$$

where EC<sub>50</sub> is the concentration of agonist that produces a half maximal response and N is the Hill slope. Proton and Zn<sup>2+</sup> inhibition curves were fitted by

$$\text{Response (\%)} = (100 - \text{minimum}) / (1 + ([\text{concentration}] / \text{IC}_{50})^N) + \text{minimum}$$

where minimum is the residual response in saturating inhibitor; for proton inhibition, the *minimum* was set to 0.

Other data are mean ± SEM. ND indicates no detectable effect of Zn<sup>2+</sup>. \*Indicates *P* < 0.05 by unpaired t-test for tau weighted, inhibition by 300 nM Zn<sup>2+</sup>, and inhibition by pH 6.8. Power to detect an effect size of 1.5 for pH, Zn<sup>2+</sup>, and P<sub>open</sub> was > 0.8. Power to detect an effect size of 2 for τ<sub>W</sub> (e.g. 20 ms change) was 0.87 (GPower 3.0).

## NMDARs containing GluN2A-S644G are gain-of-function channels with a slow response time course

We used two-electrode voltage clamp current recordings in *Xenopus laevis* oocytes to evaluate the effect of S644G on NMDAR function. GluN2A-S644G-containing NMDARs significantly increased glutamate and glycine potency (Table 1 and Supplementary Fig. 2A and B) by 17- and 11-fold, respectively. There was a significant decrease in Zn<sup>2+</sup> and H<sup>+</sup> potency, but no detectable change in voltage-dependent Mg<sup>2+</sup>-block (Table 1 and Supplementary Fig. 2C–E). We evaluated mutation effects on the deactivation time course following rapid removal of glutamate, which controls the time course of excitatory postsynaptic currents in the synapse (Lester *et al.*, 1990). Prolonged application of the endogenous agonist glutamate (in the presence of glycine) effectively causes channel opening to levels comparable between wild-type and mutant channels. Following a rapid switch from glutamate plus glycine to glycine alone, the time constant (τ) describing deactivation was significantly prolonged in the GluN2A-S644G compared to wild-type (Table 1 and Fig. 5A and B).

NMDAR open probability depends on subunit composition and varies over 50-fold (Wyllie *et al.*, 1998; Erreger *et al.*, 2005; Yuan *et al.*, 2005; Dravid *et al.*, 2008). NMDARs

containing GluN1-A652C can be irreversibly locked in the open position upon treatment with the sulphhydryl-modifying reagent methanethiosulphonate ethylammonium (MTSEA), thereby allowing for the evaluation of agonist-induced open probability (Jones *et al.*, 2002; Yuan *et al.*, 2005; Yuan *et al.*, 2009). Co-application of 200 μM MTSEA with glutamate and glycine potentiated the agonist-evoked current for wild-type NMDARs, but had minimal effects on GluN2A-S644G-containing NMDARs, suggesting a strong increase in open probability due to GluN2A-S644G (Table 1). Together, these data suggest that the S644G mutation results in a gain-of-function channel with slow deactivation kinetics.

Patients with *GRIN2A*-associated DEE typically have *de novo* heterozygous variants; thus, receptors that contain one wild-type and one variant copy of GluN2A. To investigate whether the NMDARs with one copy of GluN2A-S644G show altered function, we expressed GluN1/GluN2A<sub>C1</sub>/GluN2A<sub>C2</sub> NMDARs that contained GluN2A subunits modified by addition of coiled-coil domains and an ER retention signal on the C-terminus (Hansen *et al.*, 2014) in *Xenopus* oocytes and evaluated the concentration–response curves for glutamate and glycine. GluN1/GluN2A<sub>C1</sub>-S644G/GluN2A<sub>C2</sub> NMDARs containing one copy of the variant subunit increased the glutamate potency, as measured by reduction in the half-maximally effective concentration of agonist (EC<sub>50</sub>) from 4.7 μM to 0.8 μM. NMDARs that



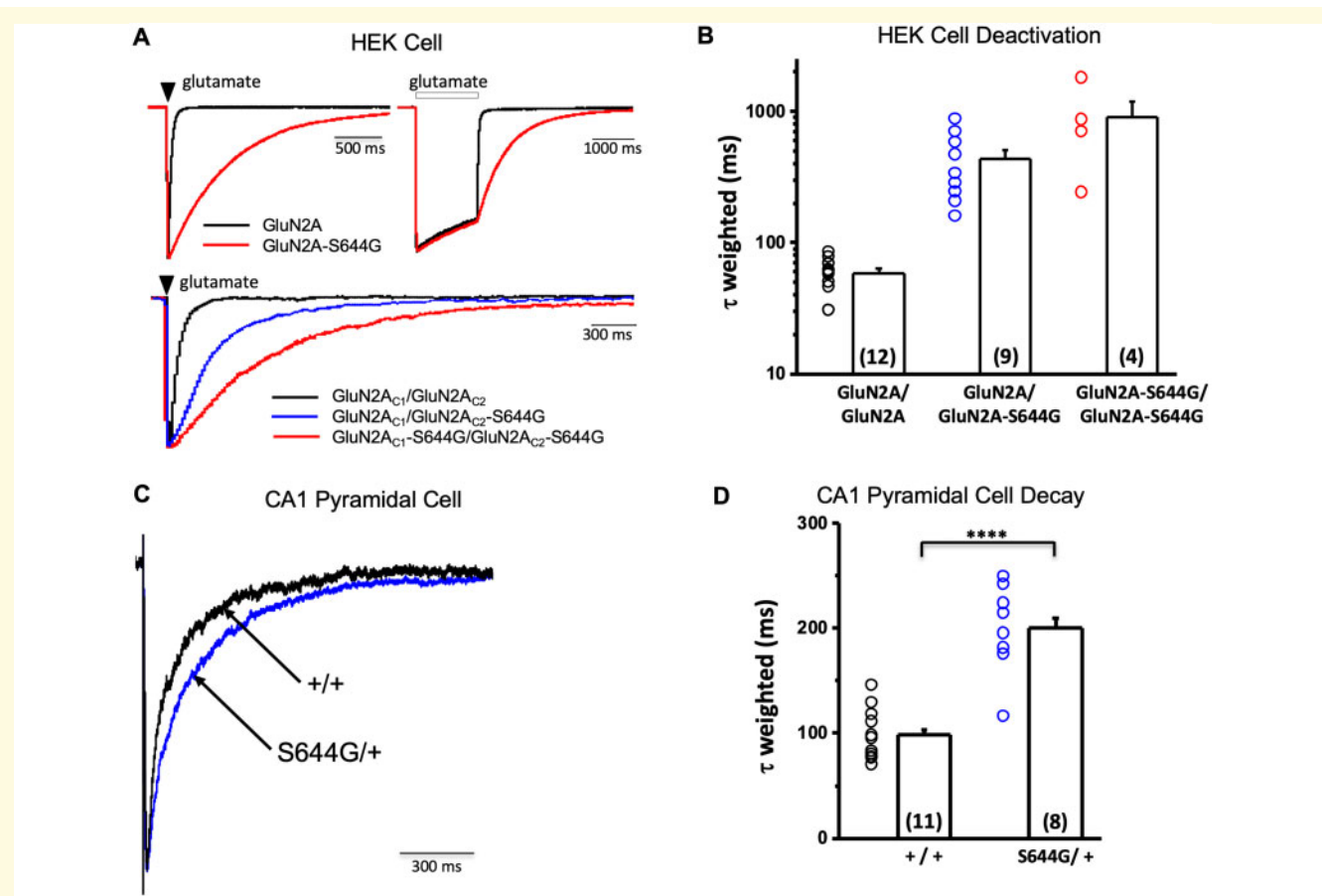


**Figure 5** GluN2A-S644G NMDAR response time course *in vitro* and synaptic time course in acute hippocampal slices. **(A)** Top: Representative GluN1/GluN2A (black) or GluN1/GluN2A-S644G (red) whole cell current time course in response to brief (1–5 ms, left) or prolonged (2 s, right) application of maximally effective concentrations of glutamate (100  $\mu$ M) and glycine (30  $\mu$ M). Bottom: The response for triheteromeric GluN1/GluN2A<sub>C1</sub>/GluN2A<sub>C2</sub> receptors that contained 0 (black), 1 (blue) or 2 (red) copies of the S644G mutation (brief pulses 20–50 ms; traces corrected for series resistance using ChannelLabv2 software) (Traynelis, 1998) (statistics are given in Table 1 and Supplementary Table 2). **(B)** Mean  $\pm$  SEM for the weighted tau describing deactivation for NMDARs expressed in HEK cells. **(C)** Superimposed, normalized evoked NMDAR-mediated component of the EPSC onto CA1 pyramidal cells in hippocampal slices from wild-type +/+ and +/S644G mice. **(D)** Mean  $\pm$  SEM for the weighted tau describing synaptic decay of the NMDAR-mediated current component of the EPSC onto CA1 pyramidal cells in +/+ (99  $\pm$  7.4 ms,  $n$  = 11 cells) and S644G/+ (200  $\pm$  15 ms,  $n$  = 8 cells) slices show a statistically significant prolongation in the S644G/+ condition (Student's two-sample  $t$ -test,  $t$  = 6.5,  $P$  = 0.0000053). The NMDAR-mediated charge transfer onto CA1 pyramidal cells was also significantly increased in the S644G/+ mouse (125  $\pm$  30 pC/pF for +/+ versus 351  $\pm$  81 pC/pF for S644G/+; Student's two-sample  $t$ -test,  $t$  = 2.93,  $P$  = 0.00935; data not shown). However, peak amplitude of the evoked EPSC was not significantly different between the two genotypes (–158 pA  $\pm$  39 pA for +/+ versus –178  $\pm$  24 pA for S644G/+; Student's two-sample  $t$ -test,  $t$  = 0.39,  $P$  = 0.71; data not shown). Other kinetic parameters of the NMDAR-mediated EPSC are as follows and were not tested for statistical significance:  $\tau_{fast}$  (49  $\pm$  6 ms for +/+ versus 100  $\pm$  9 ms for S644G/+),  $\tau_{slow}$  (266  $\pm$  35 ms for +/+ versus 1143  $\pm$  23 ms for S644G/+), % $_{fast}$  (71  $\pm$  3.3 for +/+ versus 75  $\pm$  5.1 for S644G/+), and rise time (7.1  $\pm$  0.4 ms for +/+ versus 7.6  $\pm$  0.6 ms for S644G/+). \*\*\*\* $P$  < 0.00001.

contained two copies of the variant subunit, GluN1/GluN2A<sub>C1</sub>-S644G/GluN2A<sub>C2</sub>-S644G increased the glutamate potency further to 0.09  $\mu$ M. Glycine potency was shifted in a similar manner as glutamate (Supplementary Fig. 2 and Supplementary Table 2).

Next, we used whole cell patch clamp recordings to examine the effects of synaptic expression of the GluN2A-S644G subunit in S644G/+ hippocampal brain slices. (Neurons from S644G/S644G homozygous brain slices were not possible to patch.) Monosynaptic glutamate release was initiated via Schaffer collateral stimulation, and the NMDAR-

mediated current component was isolated at –30 mV in 0.2 Mg<sup>2+</sup> via bath application of AMPAR and GABA<sub>A</sub>R antagonists (see ‘Materials and methods’ section). Although there was no difference in the peak NMDAR current response (–158 pA  $\pm$  39 pA for +/+ versus –178  $\pm$  24 pA for S644G/+; Student's two-sample  $t$ -test,  $t$  = 0.39,  $P$  = 0.71; data not shown), weighted tau, a measurement of receptor deactivation, was significantly increased by 2-fold in S644G/+ mice (99  $\pm$  7.4 ms for +/+ versus 200  $\pm$  15 ms for S644G/+; Student's two-sample  $t$ -test,  $t$  = 6.5,  $P$  = 0.0000053; Fig. 5C and D), and charge transfer was significantly increased by



2.5-fold ( $125 \pm 30$  pC/pF for  $+/+$  versus  $351 \pm 81$  pC/pF for  $S644G/+$ ; Student's two-sample  $t$ -test,  $t = 2.93$ ,  $P = 0.00935$ ; data not shown). There were no detectable changes in other measurements of NMDAR time course between  $+/+$  and  $S644G/+$  mice (detailed listing in Fig. 5 legend), and no detectable difference in membrane resistance, series resistance, or cell capacitance, or APV-sensitive leak current (data not shown, see 'Materials and methods' section). Similarly, utilizing the NMDAR expression system as described above to control subunit stoichiometry, we determined the effect of 0, 1 and 2 copies of GluN2A-S644G subunits on weighted tau ( $\tau_w$ ) in NMDARs expressed in HEK-293 cells. Our results suggest that  $\tau_w$  was significantly different for one or two copies of GluN2A-S644G compared to wild-type GluN2A ( $P < 0.05$ , one-way ANOVA, Tukey's multiple comparison test) (Supplementary Table 2 and Fig. 5A). NMDARs with a single copy of GluN2A-S644G showed a slower deactivation time course and an increase in charge transfer for responses to brief synaptic-like pulses of maximally effective concentration of glutamate compared to wild-type receptors (Supplementary Table 2). The increase in charge transfer (4-fold) was higher than that observed at

hippocampal EPSCs (2.5-fold), yet is consistent with the presence of both mutant and wild-type GluN2A-containing NMDARs, in addition to GluN2B-containing NMDARs, at the synapse in heterozygous animals. These results indicate that the synaptic NMDAR-mediated current component is significantly enhanced in  $S644G/+$  mice, in agreement with heterologous expression data.

## Hyperexcitability and abnormal network activity of *Grin2a*<sup>S644G</sup> primary neurons

We examined the effect of S644G on neuronal network hyperexcitability using MEA recording of primary cortical neurons derived from neonatal mice, recorded every other day from DIV5 to DIV29.

Early time points displayed expected low spontaneous activity and minimal network events (spikes and bursts) for all genotypes. By DIV13, networks from all genotypes had reached the maximum number of active electrodes (nAE) per well, indicating robust development of network activity

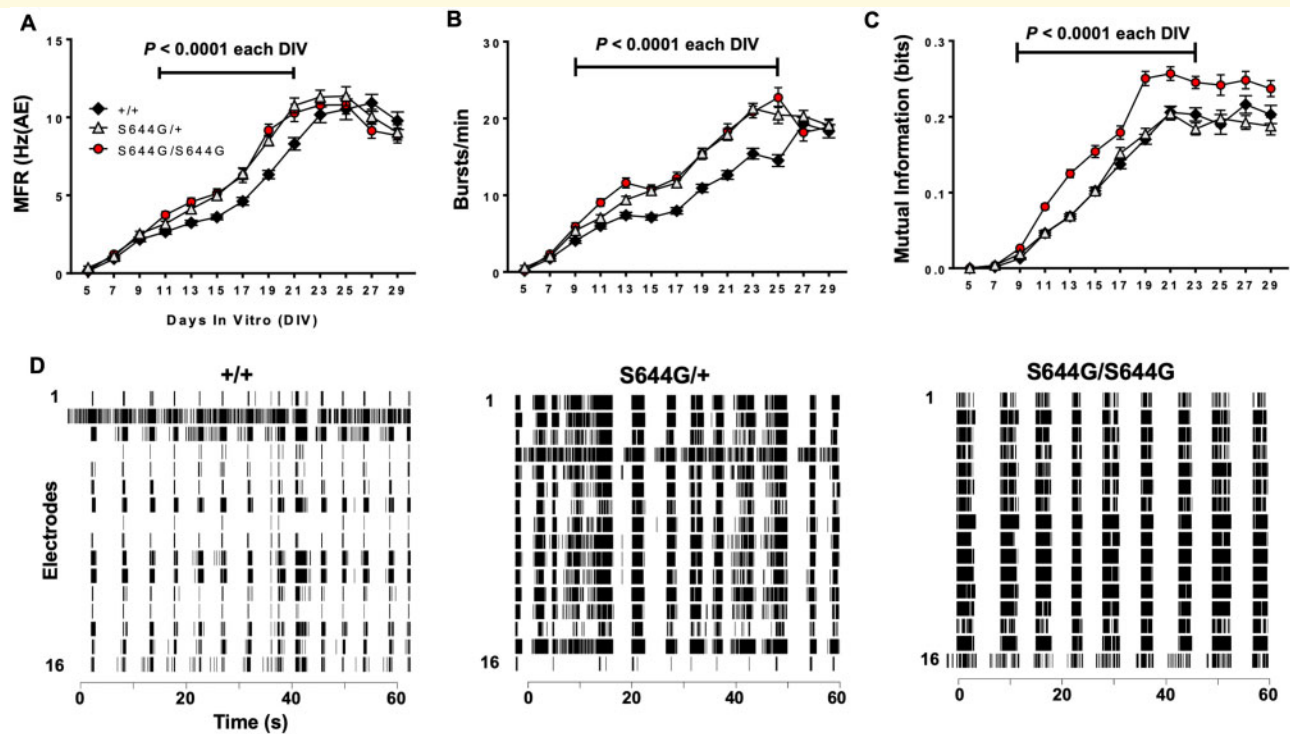


**Figure 6 MEA network phenotypes.** We analysed the activity of cortical neural networks from six litters of wild-type ( $+/+$ ,  $n = 108$  wells) and  $S644G/+$  ( $n = 107$  wells), and five litters of  $S644G/S644G$  ( $n = 80$  wells) mice. (A) Mutant neurons exhibit significantly elevated mean firing rate (MFR; expressed relative to the number of active electrodes). (B) Both mutant genotypes have a significantly higher burst rate compared to wild-type. (C)  $S644G/S644G$  networks display an increased local synchrony compared to both  $S644G/+$  and wild-type. Error bars in A–C indicate SEM. (D) Representative raster plots of network activity at DIV21 for each genotype. For statistical analysis, features from DIV9–29 were each rank- and then normal quantile-transformed and fit in a least-squares regression model using genotype and plate as covariates. The  $P$ -values obtained for genotype effect were adjusted using a Bonferroni correction for the 11 DIVs analysed for each feature. For genotype effects significant ( $P < 0.05$ ) after Bonferroni correction, a *post hoc* Dunnett's test was used ( $\alpha = 0.05$ ) to examine the effect of heterozygosity or homozygosity with wild-type as control. Supplementary Table 3 shows the genotype effect and plate effect  $P$ -values.

(Supplementary Fig. 3A). Both S644G/+ and S644G/S644G networks displayed significantly increased mean spontaneous firing rate compared to wild-type (Fig. 6A). Mutant networks also had an increased burst rate relative to wild-type (Fig. 6B).

Based on the altered bursting properties of mutant networks, we examined whether they also exhibit aberrant coordinated activity. All genotypes displayed the emergence of network bursts, which are synchronized periods of activity followed by quiescent periods (Van Pelt et al., 2004; Chiappalone et al., 2006; Wagenaar et al., 2006; Vajda et al., 2008; Cotterill et al., 2016); however, both heterozygous and homozygous networks had a significantly longer network bursts relative to wild-type (Supplementary Fig. 3B).

We investigated synchronous network firing using the mutual information algorithm, a pairwise cross-correlation of electrode activity among neighbouring electrodes that gives an indication of spatial connectivity (Gelfman et al., 2018). Mutual information analyses revealed elevated synchrony of S644G/S644G networks relative to S644G/+ or wild-type (Fig. 6C). Collectively, these data suggest that while heterozygous networks are not normal, homozygous networks have altered network topology compared to S644G/+ or wild-type. Representative raster plots highlight and summarize the network features of each genotype (Fig. 6D).

To assess activity stimulation via MEA, we treated wild-type and mutant networks with NMDA as it mimics glutamate action while being solely selective for NMDA receptors. As expected, mutant networks treated with NMDA demonstrated clearly enhanced spontaneous activity differences dependent on gene dosage such that S644G/S644G networks exhibited significantly higher firing rates than S644G/+ networks, which were themselves significantly more sensitive than wild-type (Supplementary Fig. 3); this increased excitability by subsaturating NMDA is consistent with the increase agonist potency observed for the S644G-containing receptor. Activity declined in all genotypes at higher doses of NMDA with mutants being more strongly affected. Network responses to agonist were further probed using electrical stimulation (see 'Materials and methods' section). Electrical stimulation in the presence of exogenous NMDA resulted in sustained activity of S644G/S644G networks compared to wild-type (Supplementary Fig. 3D). Administration of NMDA to wild-type networks did not result in an increased evoked response duration further demonstrating that homozygous networks possess enhanced susceptibility to agonist, which likely causes the mutant hyperactivity and altered bursting properties. Overall, the MEA studies suggest that the seizure phenotypes observed *in vivo* correlate with robust, quantifiable phenotypes in cultured neuronal networks.

## Prospects of NMDAR antagonist combination therapy

The initial seizure frequency in the *GRIN2A* S644G patient was ~200 per month, with no seizure-free days (Fig. 7A).

Prior to a genetic diagnosis, empirical treatment trials with vigabatrin, topiramate, levetiracetam, and clobazam were unsuccessful in reducing seizures. After the genetic diagnosis, treatment with the NMDAR antagonist memantine was considered as a rational candidate because of reports of this agent's efficacy and safety in children with other *GRIN2A* gain-of-function variants (Hosenbocus and Chahal, 2013; Pierson et al., 2014; Nguyen et al., 2016). Given our functional data supporting a gain-of-function effect and the effectiveness of memantine *in vitro* (see below and Fig. 7A), treatment with memantine began at age 2 years and following treatment, the daily seizure burden was reduced by half. This was followed by treatment with dextromethorphan, another NMDAR antagonist used safely for other indications in children, at age 3 years at doses of 5 mg/kg/day increasing to 10 mg/kg/day. While there was not substantial additional benefit, we observed some worsening of seizures with attempts to wean from dextromethorphan. The patient, now 6.5 years old, experiences three to five brief tonic seizures and one to two myoclonic seizures per day on a combination of memantine, dextromethorphan, and zonisamide (Fig. 7A). Profound intellectual disability, spastic quadriplegia, cortical visual impairment and oropharyngeal dysphasia persist.

Exploiting the viability of *Xenopus laevis* oocytes expressing the mutant channel, NMDAR drug candidates were tested and efficacy in half-maximal inhibitory responses was assessed. Different classes of NMDAR antagonists inhibited channel activation with modestly reduced potency compared to wild-type receptors (Supplementary Fig. 2F and G). Because neurons express receptors that contain one copy of the mutant allele, we expressed receptors in which we could control subunit stoichiometry using coiled-coil domain masking of an ER-retention signal. Supplementary Fig. 2 shows the properties of the receptors, and Fig. 7B and C shows the potency of two FDA-approved drugs (memantine and dextromethorphan). The inhibitory effects of memantine and dextromethorphan were corroborated in cortical networks on MEA (Fig. 7D and E). Together, these data encouraged us to test whether NMDAR antagonists would mitigate lethal seizures of S644G homozygous pups.

In a first trial, homozygous pups were treated with dextromethorphan from postnatal Day 8 to 21 at the established ED<sub>50</sub> of 25 mg/kg (Kim et al., 2003). Dextromethorphan extended the survival of homozygous pups by a 1-day median (Fig. 7E;  $P = 0.002$ , Mantel-Cox log-rank test). To improve the exposure of dextromethorphan, we tried Nuedexta<sup>®</sup>, a combination drug that is composed of dextromethorphan (25 mg/kg) and quinidine (10 mg/kg), with the rationale to extend the half-life and potentially increase exposure of dextromethorphan because quinidine at low concentration is known to block the rapid metabolism of dextromethorphan to dextroprhan, a more potent but short-lived metabolite (Pioro et al., 2010). Nuedexta<sup>®</sup> treatment of *Grin2a*<sup>S644G</sup> homozygotes extended pup survival significantly further than

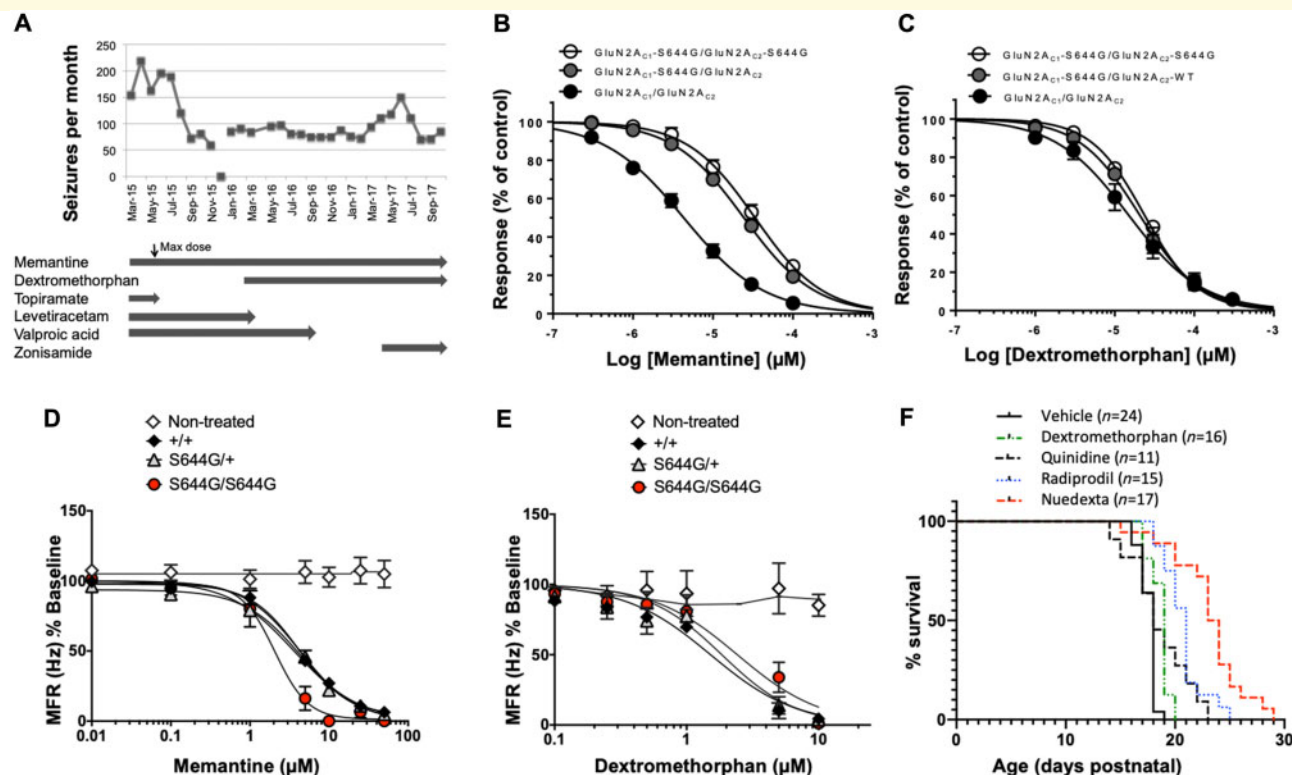


**Figure 7** Impact of drug therapy on clinical seizures, *in vitro*, on network hyperexcitability in neurons and on lethal seizures in mice. (**A** and **B**) Composite concentration-response curves for memantine ( $n = 1\text{--}12$  oocytes) and dextromethorphan ( $n = 10\text{--}13$  oocytes) on NMDA receptors that contained 0, 1, or 2 mutant GluN2A-S644G subunits. The  $\text{IC}_{50}$  values for single and double copy GluN2A-S644G mutant receptors for both dextromethorphan and memantine were significantly different from wild-type GluN2A receptors ( $P < 0.05$ , ANOVA and Neuman-Kuels multiple comparison test). (**C** and **D**) Fitted concentration-response curves for memantine and dextromethorphan on MEA. Data for each well are normalized to baseline firing collected before treatment. Memantine;  $n = 3$  litters for wild-type and S644G + ( $\geq 21$  wells each concentration),  $n = 1$  litter for S644G/S644G (four wells each concentration). Dextromethorphan;  $n = 5$  litters for wild-type and S644G/+ ( $\geq 22$  wells each concentration), and two litters for S644G/S644G (12 wells each concentration). Non-treated controls; 42 and 24 wells memantine and dextromethorphan, respectively. Compound  $\text{IC}_{50}$  values are shown in [Supplementary Table 2](#). Genotype  $\times$  treatment interaction effects were tested in a least-squares regression model of rank- and then normal quantile-transformed data. (**E**) Pharmacological rescue of lethal seizures of S644G/S644G homozygotes, showing the respective survival after daily injections of dextromethorphan, quinidine, radiprodil, and Nuedexta<sup>®</sup>. The respective doses were chosen to be just under known toxic doses in mice. The Mantel-Cox log-rank test was used to determine significant differences between curves: vehicle versus dextromethorphan (+1 day median survival,  $\chi^2 = 13.8$ ,  $P < 0.0002$ ); vehicle versus radiprodil (+3 days,  $\chi^2 = 29.1$ ,  $P < 0.0001$ ); vehicle versus Nuedexta<sup>®</sup> (+5.5 days,  $\chi^2 = 29.8$ ,  $P < 0.0001$ ); vehicle versus quinidine (+1 day median survival,  $\chi^2 = 3.69$ ,  $P = 0.055$ ).

dextromethorphan alone, by a median of 5.5 days (Fig. 7E;  $P < 0.0001$ , Mantel-Cox log-rank test), while quinidine alone only modestly extended survival by a median of 1 day (Fig. 7E;  $P < 0.02$ , Mantel-Cox log-rank test). Because *Grin2a*<sup>S644G</sup> show overactive NMDAR currents, we also tested radiprodil (2 mg/kg), as it blocks a different population of GluN2B-containing NMDARs (Borza and Domany, 2006; Mony *et al.*, 2009). Radiprodil extended survival by 3 days, further than dextromethorphan alone, but not as long as Nuedexta<sup>®</sup> (Fig. 7E;  $P < 0.0001$ , Mantel-Cox log-rank test). Although the severe seizures of S644G homozygotes do offer a very robust challenge for testing therapeutic intervention, these results support further investigation into NMDAR antagonist therapies.

## Discussion

The *GRIN2A* S644G substitution in a patient with DEE, modelled in our studies, resides in the highly conserved signature gating sequence (SYTANLAAF) in TM3, the third transmembrane pore region of the NMDAR. Amongst all variants examined in heterologous systems, it displays one of the strongest gain-of-function effects on channel activity. *Grin2a*<sup>S644G</sup> mutant mice were developed as part of a larger effort to model the pathophysiological features of children with DEE due to gain-of-function GRIN gene variants, and in which to explore therapies. The key features of *GRIN2A*-associated DEE are medically refractory epilepsy, including infantile spasms, and developmental delay/intellectual disability. *Grin2a*<sup>S644G</sup> mice mimic several aspects of human



disease, including seizure susceptibility, distinct neurobehavioural features and a reduction of hippocampal size; the latter has not yet been described in *GRIN2A* DEE, but other NMDAR genetic variants are accompanied by other forms of neuroanatomical abnormality (Platzer et al., 2017; Fry et al., 2018). Previously *Grin2a* null mice were described with developmental and sleep abnormalities and modest epileptiform activity (Salmi et al., 2018; Salmi et al., 2019), but *Grin2a*<sup>S644G</sup> is the first described example of NMDAR gain-of-function variant with epilepsy in an animal model.

While we observed some expected phenotypes in *Grin2a*<sup>S644G</sup> mice overall, our study suggests a biologically very complex disease. Depending on mutant gene dosage and seizure assessment, *Grin2a*<sup>S644G</sup> mice are both seizure-susceptible (spontaneous lethal seizures; low threshold to electroconvulsive minimal and maximal seizure end points) and seizure-resistant (elevated threshold to electroconvulsive partial seizures; relative resistance to PTZ-induced tonic-clonic seizures). Given the breadth and extent of *Grin2a* expression in the brain, we strongly suspect these differences stem from pleiotropy in different neuron types and brain regions, as has been suggested or shown directly with the advent of conditional mutations in other mouse seizure models (Papale et al., 2009; Wagnon et al., 2011; Asinof et al., 2015; Makinson et al., 2016). Pleiotropy is not unexpected for widely and highly expressed genes such as *Grin2a* and likely contributes to the diversity of co-morbid behaviours, as shown previously for *Dnm1*<sup>F<sup>fl</sup></sup>, the mouse model of *DNM1* EE (Asinof et al., 2015), although the opposing seizure-related characteristics of *Grin2a*<sup>S644G</sup> suggest further biological complexities.

NMDAR gene variants, including those in *GRIN2A*, are associated with autism spectrum disorder (Yuan et al., 2015) and aphasia (Carvill et al., 2013), and *GRIN2A* has recently been implicated in attention deficit hyperactivity disorder (Slopien et al., 2006). The features in *Grin2a*<sup>S644G</sup> heterozygous mice of hyperactivity, decreased anxiety, and stereotypies are consistent with the human disease spectrum (Hu et al., 2016). Notably, in our patient and in many with DEE, the level of cognitive function is sufficiently low to preclude reliable anxiety measurements. We also note that our patient with *GRIN2A* S644G showed no evidence of hyperactivity or stereotypies. However, in many genetic DEEs there can be significant phenotypic heterogeneity among patients with the same primary gene defect—even when harbouring the identical variant (Helbig and Tayoun, 2016)—which, when also considering the many genetic differences across and within species, warrants caution about attempting to cross-correlate phenotypes too narrowly.

Nevertheless, rodent models offer unique advantages to probe vulnerabilities at the circuit and cellular level caused by the orthologous genetic defect. Specifically, the relative resistance of *Grin2a*<sup>S644G</sup> heterozygotes to 6 Hz partial seizures suggests altered limbic system function or connectivity (Barton et al., 2001; Metcalf et al., 2017). Ironically, vulnerability in the limbic system is also suggested by the lethal seizures whose features include a wild run followed rapidly

by tonic-clonic episodes and tonic hindlimb extension, resembling audiogenic seizures that are known to involve paroxysmal activity in the cortex, medial geniculate, hippocampus, and amygdala (Marescaux et al., 1987; Naritoku et al., 1992; Dutra Moraes et al., 2000; Faingold, 2012); the main structures of limbic circuitry (Giordano et al., 2015, 2016). Furthermore, the relative resistance of *Grin2a*<sup>S644G</sup> heterozygotes to tonic-clonic seizures induced by the GABA<sub>A</sub>R antagonist PTZ, whilst retaining sensitivity to generalized electroconvulsion, suggest deficits in GABAergic neurons. Interestingly, mice lacking the excitatory postsynapse scaffold protein IQSEC2, which also exhibit lethal spontaneous seizures and seizure resistance in 6 Hz ECT and PTZ tests, have increased excitatory drive onto hippocampal interneurons and altered intrinsic hippocampal interneuron properties (Sah et al., 2020). The two models compared suggest possible convergence of mechanisms of genetically diverse DEE's, which might help in identifying common therapies—invaluable given the extensive genetic heterogeneity of DEE.

Functional characterization of mutant channel activity shows a very strong gain-of-function effect and slower kinetics, supported by assessment of synaptic activity in excitatory neurons of mutant mice. Evaluation of receptors with zero, one or two copies of the mutant allele revealed an intermediate effect of S644G when only one copy of the variant is present in the complex. Although the synaptic data indicate a prolongation of NMDAR-mediated current and an increase in charge transfer in the mutants, the results—while significant—were less striking than in heterologous assays. Several potential explanations for this exist, including likely binomial probability of receptors having receptors with zero, one or two copies of the mutant, and wild-type subunits will confer faster synaptic time course. In addition, some receptors at this age will contain two copies of GluN2B in the synapse. Tri-heteromeric NMDARs that contain one GluN2B subunit and one GluN2A-S644G subunit may also reside in the synapse since both GluN2A and GluN2B expression are high in excitatory pyramidal cells in developing mice (Monyer et al., 1994; Hansen et al., 2014). There also may be systematic bias towards healthy neurons that allowed stable patch clamp recording, which may have selected against cells with strong expression of GluN2A-S644G.

MEA examination of activity patterns in mutant primary neurons and their longitudinal study during network establishment revealed the development of hyperactive mutant networks. S644G heterozygotes and homozygotes have similar mean firing rates and bursting features, perhaps reflecting more cell-autonomous effects, but homozygotes stand out in more complex measures of network synchronicity.

The presence of quantifiable excitability features and the mirroring of pharmacological rescue of aberrant activity by NMDAR antagonists prior to laborious *in vivo* testing represent significant opportunities for preclinical intervention screening. Screening therapeutic compounds in both *in vitro* and *ex vivo* platforms should identify compounds with



better efficacy than in either alone. The prominent lethal seizures of homozygous mutants also afford a robust challenge to explore the potential of NMDAR antagonists as therapeutic agents. Although the homozygous S644G mice eventually succumbed to lethal seizures irrespective of treatment regimen, the extension of survival by 5.5 days (or 30% of their lifespan) by using Nuedexta<sup>®</sup> is an indication that further studies of NMDAR targeted therapies are warranted.

## Acknowledgements

We are grateful to our patient's family for participating in our research to allow for sharing of de-identified data. We would like to thank Sophie Colombo and Sahar Gelfman for helpful discussions regarding MEA analyses, and Aamir Zuberi for his help in generating the mouse model.

## Funding

National Institutes of Health (US) grant NS031348 (W.N.F.), National Institutes of Health (US) grant OD020351 (W.N.F., C.M.L., D.B.G.), National Institutes of Health (US) grant HD082373 (H.Y.), National Institutes of Health (US) grants NS065371, NS111619 and NS092989 (S.F.T.), Boston Children's Hospital Translational Research Program (A.P.), W.H. (Chinese Scholars Council), W.C. (Xiangya-Emory Medical Schools Visiting Student Program), American Epilepsy Society Fellowship 564945 (S.B.), CURE (S.F.T.). The funding agencies did not participate in the design or execution of the study.

## Competing interests

S.F.T. is a PI on research grants from Allergan, Biogen and Janssen to Emory University School of Medicine, is a paid consultant for Janssen, is a member of the SAB for Sage Therapeutics, is co-founder of NeurOp Inc, and receives royalties for software. S.F.T. is co-inventor on Emory-owned Intellectual Property that includes allosteric modulators of NMDA receptor function. H.Y. is PI on a research grant from Sage Therapeutics to Emory University School of Medicine. D.B.G. is a founder of and holds equity in Praxis, serves as a consultant to AstraZeneca, and has received research support from Janssen, Gilead, Biogen, AstraZeneca and UCB.

## Supplementary material

Supplementary material is available at *Brain* online.

## References

- Akazawa C, Shigemoto R, Bessho Y, Nakanishi S, Mizuno N. Differential expression of five N-methyl-D-aspartate receptor subunit mRNAs in the cerebellum of developing and adult rats. *J Comp Neurol* 1994; 347: 150–60.
- Asinof S, Mahaffey C, Beyer B, Frankel WN, Boumil R. Dynamin 1 isoform roles in a mouse model of severe childhood epileptic encephalopathy. *Neurobiol Dis* 2016; 95: 1–11.
- Asinof SK, Sukoff Rizzo SJ, Buckley AR, Beyer BJ, Letts VA, Frankel WN, et al. Independent neuronal origin of seizures and behavioral comorbidities in an animal model of a severe childhood genetic epileptic encephalopathy. *PLoS Genet* 2015; 11: e1005347.
- Bar-Shira O, Maor R, Chechik G. Gene expression switching of receptor subunits in human brain development. *PLoS Comput Biol* 2015; 11: e1004559.
- Barton ME, Klein BD, Wolf HH, White HS. Pharmacological characterization of the 6 Hz psychomotor seizure model of partial epilepsy. *Epilepsy Res* 2001; 47: 217–27.
- Borza I, Domany G. NR2B selective NMDA antagonists: the evolution of the ifenprodil-type pharmacophore. *Curr Top Med Chem* 2006; 6: 687–95.
- Carvill GL, Regan BM, Yendle SC, O'Roak BJ, Lozovaya N, Bruneau N, et al. *GRIN2A* mutations cause epilepsy-aphasia spectrum disorders. *Nat Genet* 2013; 45: 1073–6.
- Chen C, Okayama H. High-efficiency transformation of mammalian cells by plasmid DNA. *Mol Cell Biol* 1987; 7: 2745–52.
- Chen W, Tankovic A, Burger PB, Kusumoto H, Traynelis SF, Yuan H. Functional evaluation of a de novo *GRIN2A* mutation identified in a patient with profound global developmental delay and refractory epilepsy. *Mol Pharmacol* 2017; 91: 317–30.
- Chiappalone M, Bove M, Vato A, Tedesco M, Martinoia S. Dissociated cortical networks show spontaneously correlated activity patterns during in vitro development. *Brain Res* 2006; 1093: 41–53.
- Cotterill E, Charlesworth P, Thomas CW, Paulsen O, Eglén SJ. A comparison of computational methods for detecting bursts in neuronal spike trains and their application to human stem cell-derived neuronal networks. *J Neurophysiol* 2016; 116: 306–21.
- de Ligt J, Willemsen MH, van Bon BW, Kleefstra T, Yntema HG, Kroes T, et al. Diagnostic exome sequencing in persons with severe intellectual disability. *N Engl J Med* 2012; 367: 1921–9.
- Dravid SM, Prakash A, Traynelis SF. Activation of recombinant NR1/NR2C NMDA receptors. *J Physiol* 2008; 586: 4425–39.
- Dutra Moraes MF, Galvis-Alonso OY, Garcia-Cairasco N. Audiogenic kindling in the Wistar rat: a potential model for recruitment of limbic structures. *Epilepsy Res* 2000; 39: 251–9.
- Endele S, Rosenberger G, Geider K, Popp B, Tamer C, Stefanova I, et al. Mutations in *GRIN2A* and *GRIN2B* encoding regulatory subunits of NMDA receptors cause variable neurodevelopmental phenotypes. *Nat Genet* 2010; 42: 1021–6.
- Erreger K, Dravid SM, Banke TG, Wyllie DJ, Traynelis SF. Subunit-specific gating controls rat NR1/NR2A and NR1/NR2B NMDA channel kinetics and synaptic signalling profiles. *J Physiol* 2005; 563: 345–58.
- Faingold CL. Brainstem networks: reticulo-cortical synchronization in generalized convulsive seizures. In: JL Noebels, M Avoli, MA Rogawski, RW Olsen, AV Delgado-Escueta, editors. *Jasper's basic mechanisms of the epilepsies*, 4th edn. Bethesda, MD: National Center for Biotechnology Information; 2012.
- Fry AE, Fawcett KA, Zelnik N, Yuan H, Thompson BAN, Shemer-Meiri L, et al. De novo mutations in *GRIN1* cause extensive bilateral polymicrogyria. *Brain* 2018; 141: 698–712.
- Gelfman S, Wang Q, Lu YF, Hall D, Bostick CD, Dhindsa R, et al. meaRtools: an R package for the analysis of neuronal networks recorded on microelectrode arrays. *PLoS Comput Biol* 2018; 14: e1006506.

- Giordano C, Costa AM, Lucchi C, Leo G, Brunel L, Fehrentz JA, et al. Progressive seizure aggravation in the repeated 6-hz corneal stimulation model is accompanied by marked increase in hippocampal p-ERK1/2 immunoreactivity in neurons. *Front Cell Neurosci* 2016; 10: 281.
- Giordano C, Vinet J, Curia G, Biagini G. Repeated 6-Hz corneal stimulation progressively increases FosB/DeltaFosB levels in the lateral amygdala and induces seizure generalization to the hippocampus. *PLoS One* 2015; 10: e0141221.
- Grea H, Scheid I, Gaman A, Rogemond V, Gillet S, Honnorat J, et al. Clinical and autoimmune features of a patient with autism spectrum disorder seropositive for anti-NMDA-receptor autoantibody. *Dialogues Clin Neurosci* 2017; 19: 65–70.
- Hacohen Y, Wright S, Gadian J, Vincent A, Lim M, Wassmer E, et al. N-methyl-D-aspartate (NMDA) receptor antibodies encephalitis mimicking an autistic regression. *Dev Med Child Neurol* 2016; 58: 1092–4.
- Hamdan FF, Gauthier J, Araki Y, Lin DT, Yoshizawa Y, Higashi K, et al. Excess of de novo deleterious mutations in genes associated with glutamatergic systems in nonsyndromic intellectual disability. *Am J Hum Genet* 2011; 88: 306–16.
- Hansen KB, Ogdan KK, Yuan H, Traynelis SF. Distinct functional and pharmacological properties of triheteromeric GluN1/GluN2A/GluN2B NMDA receptors. *Neuron* 2014; 81: 1084–96.
- Helbig I, Tayoun AA. Understanding genotypes and phenotypes in epileptic encephalopathies. *Mol Syndromol* 2016; 7: 172–81.
- Hosenbocus S, Chahal R. Memantine: a review of possible uses in child and adolescent psychiatry. *J Can Acad Child Adolesc Psychiatry* 2013; 22: 166–71.
- Hu C, Chen W, Myers SJ, Yuan H, Traynelis SF. Human GRIN2B variants in neurodevelopmental disorders. *J Pharmacol Sci* 2016; 132: 115–21.
- Johnstone AF, Gross GW, Weiss DG, Schroeder OH, Gramowski A, Shafer TJ. Microelectrode arrays: a physiologically based neurotoxicity testing platform for the 21st century. *Neurotoxicology* 2010; 31: 331–50.
- Jones KS, VanDongen HM, VanDongen AM. The NMDA receptor M3 segment is a conserved transduction element coupling ligand binding to channel opening. *J Neurosci* 2002; 22: 2044–53.
- Kim HC, Shin CY, Seo DO, Jhoo JH, Jhoo WK, Kim WK, et al. New morphinan derivatives with negligible psychotropic effects attenuate convulsions induced by maximal electroshock in mice. *Life Sci* 2003; 72: 1883–95.
- Kim S, Kim DG, Gonzales EL, Mabunga DFN, Shin D, Jeon SJ, et al. Effects of intraperitoneal N-methyl-D-aspartate (NMDA) administration on nociceptive/repetitive behaviors in juvenile mice. *Biomol Ther (Seoul)* 2019; 27: 168–77.
- Lee EJ, Lee H, Huang TN, Chung C, Shin W, Kim K, et al. Trans-synaptic zinc mobilization improves social interaction in two mouse models of autism through NMDAR activation. *Nat Commun* 2015; 6: 7168.
- Lesca G, Rudolf G, Bruneau N, Lozovaya N, Labalme A, Boutry-Kryza N, et al. GRIN2A mutations in acquired epileptic aphasia and related childhood focal epilepsies and encephalopathies with speech and language dysfunction. *Nat Genet* 2013; 45: 1061–6.
- Lester RA, Clements JD, Westbrook GL, Jahr CE. Channel kinetics determine the time course of NMDA receptor-mediated synaptic currents. *Nature* 1990; 346: 565–7.
- Mack CM, Lin BJ, Turner JD, Johnstone AF, Burgoon LD, Shafer TJ. Burst and principal components analyses of MEA data for 16 chemicals describe at least three effects classes. *Neurotoxicology* 2014; 40: 75–85.
- Makinson CD, Dutt K, Lin F, Papale LA, Shankar A, Barela AJ, et al. An Scn1a epilepsy mutation in Scn8a alters seizure susceptibility and behavior. *Exp Neurol* 2016; 275 (Pt 1): 46–58.
- Marescaux C, Vergnes M, Kiesmann M, Depaulis A, Micheletti G, Warter JM. Kindling of audiogenic seizures in Wistar rats: an EEG study. *Exp Neurol* 1987; 97: 160–8.
- Metcalf CS, West PJ, Thomson KE, Edwards SF, Smith MD, White HS, et al. Development and pharmacologic characterization of the rat 6 Hz model of partial seizures. *Epilepsia* 2017; 58: 1073–84.
- Mony L, Kew JN, Gunthorpe MJ, Paoletti P. Allosteric modulators of NR2B-containing NMDA receptors: molecular mechanisms and therapeutic potential. *Br J Pharmacol* 2009; 157: 1301–17.
- Monyer H, Burnashev N, Laurie DJ, Sakmann B, Seeburg PH. Developmental and regional expression in the rat brain and functional properties of four NMDA receptors. *Neuron* 1994; 12: 529–40.
- Myers SJ, Yuan H, Kang JQ, Tan FCK, Traynelis SF, Low CM. Distinct roles of GRIN2A and GRIN2B variants in neurological conditions. *F1000Res* 2019; 8. doi: 10.12688/f1000research.18949.1.
- Naritoku DK, Mecozzi LB, Aiello MT, Faingold CL. Repetition of audiogenic seizures in genetically epilepsy-prone rats induces cortical epileptiform activity and additional seizure behaviors. *Exp Neurol* 1992; 115: 317–24.
- Nguyen L, Thomas KL, Lucke-Wold BP, Cavendish JZ, Crowe MS, Matsumoto RR. Dextromethorphan: an update on its utility for neurological and neuropsychiatric disorders. *Pharmacol Ther* 2016; 159: 1–22.
- Novellino A, Scelfo B, Palosaari T, Price A, Sobanski T, Shafer TJ, et al. Development of micro-electrode array based tests for neurotoxicity: Assessment of interlaboratory reproducibility with neuroactive chemicals. *Front Neuroeng* 2011; 4: 4. doi: 10.3389/fneng.2011.00004.
- Ogden KK, Chen W, Swanger SA, McDaniel MJ, Fan LZ, Hu C, et al. Molecular mechanism of disease-associated mutations in the pre-M1 helix of NMDA receptors and potential rescue pharmacology. *PLoS Genet* 2017; 13: e1006536.
- Otso N. A threshold selection method from gray-level histograms. *Automatica* 1975; 11: 23–7.
- Paoletti P, Bellone C, Zhou Q. NMDA receptor subunit diversity: impact on receptor properties, synaptic plasticity and disease. *Nat Rev Neurosci* 2013; 14: 383–400.
- Papale LA, Beyer B, Jones JM, Sharkey LM, Tufik S, Epstein M, et al. Heterozygous mutations of the voltage-gated sodium channel SCN8A are associated with spike-wave discharges and absence epilepsy in mice. *Hum Mol Genet* 2009; 18: 1633–41.
- Petrovski S, Kwan P. Unraveling the genetics of common epilepsies: approaches, platforms, and caveats. *Epilepsy Behav* 2013; 26: 229–33.
- Pierson TM, Yuan H, Marsh ED, Fuentes-Fajardo K, Adams DR, Markello T, et al. GRIN2A mutation and early-onset epileptic encephalopathy: personalized therapy with memantine. *Ann Clin Transl Neurol* 2014; 1: 190–8.
- Pioro EP, Brooks BR, Cummings J, Schiffer R, Thisted RA, Wynn D, et al. Dextromethorphan plus ultra low-dose quinidine reduces pseudobulbar affect. *Ann Neurol* 2010; 68: 693–702.
- Platzer K, Yuan H, Schutz H, Winschel A, Chen W, Hu C, et al. GRIN2B encephalopathy: novel findings on phenotype, variant clustering, functional consequences and treatment aspects. *J Med Genet* 2017; 54: 460–70.
- Racine RJ. Modification of seizure activity by electrical stimulation. II. Motor seizure. *Electroencephalogr Clin Neurophysiol* 1972; 32: 281–94.
- Rossi M, Chatron N, Labalme A, Ville D, Carneiro M, Ederly P, et al. Novel homozygous missense variant of GRIN1 in two sibs with intellectual disability and autistic features without epilepsy. *Eur J Hum Genet* 2017; 25: 376–80.
- Sah M, Shore A, Petri S, Kanber A, Yang M, Weston MC, et al. Altered excitatory transmission onto hippocampal interneurons in the IQSEC2 mouse model of X-linked neurodevelopmental disease. *Neurobiol Dis* 2020; 137: 104758. doi: 10.1016/j.nbd.2020.104758.
- Salmi M, Bolbos R, Bauer S, Minlebaev M, Burnashev N, Szepietowski P. Transient microstructural brain anomalies and epileptiform

- discharges in mice defective for epilepsy and language-related NMDA receptor subunit gene *Grin2a*. *Epilepsia* 2018; 59: 1919–30.
- Salmi M, Del Gallo F, Minlebaev M, Zakharov A, Pauly V, Perron P, et al. Impaired vocal communication, sleep-related discharges, and transient alteration of slow-wave sleep in developing mice lacking the *GluN2A* subunit of N-methyl-D-aspartate receptors. *Epilepsia* 2019; 60: 1424–37.
- Shahaf G, Marom S. Learning in networks of cortical neurons. *J Neurosci* 2001; 21: 8782–8.
- Slopien A, Dmitrzak-Weglaz M, Rybakowski F, Rajewski A, Hauser J. [Genetic background of ADHD: genes of the serotonergic system, other candidate genes, endophenotype. *Psychiatr Pol* 2006; 40: 33–42.
- Strehlow V, Heyne HO, Vlaskamp DRM, Marwick KFM, Rudolf G, de Bellescize J, et al. *GRIN2A*-related disorders: genotype and functional consequence predict phenotype. *Brain* 2019; 142: 80–92.
- Traynelis SF. Software-based correction of single compartment series resistance errors. *J Neurosci Methods* 1998; 86: 25–34.
- Traynelis SF, Wollmuth LP, McBain CJ, Menniti FS, Vance KM, Ogden KK, et al. Glutamate receptor ion channels: structure, regulation, and function. *Pharmacol Rev* 2010; 62: 405–96.
- Vajda I, van Pelt J, Wolters P, Chiappalone M, Martinoia S, van Someren E, et al. Low-frequency stimulation induces stable transitions in stereotypical activity in cortical networks. *Biophys J* 2008; 94: 5028–39.
- Van Pelt J, Corner MA, Wolters PS, Rutten WL, Ramakers GJ. Long-term stability and developmental changes in spontaneous network burst firing patterns in dissociated rat cerebral cortex cell cultures on multielectrode arrays. *Neurosci Lett* 2004; 361: 86–9.
- Wagenaar DA, Pine J, Potter SM. Effective parameters for stimulation of dissociated cultures using multi-electrode arrays. *J Neurosci Methods* 2004; 138: 27–37.
- Wagenaar DA, Pine J, Potter SM. An extremely rich repertoire of bursting patterns during the development of cortical cultures. *BMC Neurosci* 2006; 7: 11.
- Wagenaar DA, Potter SM. A versatile all-channel stimulator for electrode arrays, with real-time control. *J Neural Eng* 2004; 1: 39–45.
- Wagnon JL, Mahaffey CL, Sun W, Yang Y, Chao HT, Frankel WN. Etiology of a genetically complex seizure disorder in *Celf4* mutant mice. *Genes Brain Behav* 2011; 10: 765–77.
- Wyllie DJ, Behe P, Colquhoun D. Single-channel activations and concentration jumps: comparison of recombinant NR1a/NR2A and NR1a/NR2D NMDA receptors. *J Physiol* 1998; 510: 1–18.
- XiangWei W, Jiang Y, Yuan H. De novo mutations and rare variants occurring in NMDA receptors. *Curr Opin Physiol* 2018; 2: 27–35.
- Yang M, Bozdagi O, Scattoni ML, Wohr M, Rouillet FI, Katz AM, et al. Reduced excitatory neurotransmission and mild autism-relevant phenotypes in adolescent *Shank3* null mutant mice. *J Neurosci* 2012; 32: 6525–41.
- Yuan H, Erreger K, Dravid SM, Traynelis SF. Conserved structural and functional control of N-methyl-D-aspartate receptor gating by transmembrane domain M3. *J Biol Chem* 2005; 280: 29708–16.
- Yuan H, Hansen KB, Vance KM, Ogden KK, Traynelis SF. Control of NMDA receptor function by the NR2 subunit amino-terminal domain. *J Neurosci* 2009; 29: 12045–58.
- Yuan H, Hansen KB, Zhang J, Pierson TM, Markello TC, Fajardo KV, et al. Functional analysis of a de novo *GRIN2A* missense mutation associated with early-onset epileptic encephalopathy. *Nat Commun* 2014; 5: 3251.
- Yuan H, Low CM, Moody OA, Jenkins A, Traynelis SF. Ionotropic GABA and glutamate receptor mutations and human neurologic disease. *Mol Pharmacol* 2015; 88: 203–17.